LAWRENCE
LIVERMORE
NATIONAL
LABORATORY

UCRL-TR-212566

Chemical Environment at Waste Package Surfaces in a High-Level Radioactive Waste Repository

S. Carroll, M. Alai, L. Craig, G. Gdowski, P. Hailey,
Q. A. Nguyen, J. Rard, K. Staggs, M. Sutton, T. Wolery

May 26, 2005

This work was performed under the auspices of the U.S. Department of Energy by University of California, Lawrence Livermore National Laboratory under Contract W-7405-Eng-48.

Chemical Environment at Waste Package Surfaces in a High-Level Radioactive Waste Repository

Susan Carroll[1], Maureen Alai, Laura Craig, Greg Gdowski, Phil Hailey, Que Anh Nguyen, Joe Rard, Kirk Staggs, Mark Sutton, Tom Wolery
Lawrence Livermore National Laboratory
Livermore, CA 94550
UCRL-TR-212566

Summary
We have conducted a series of deliquescence, boiling point, chemical transformation, and evaporation experiments to determine the composition of waters likely to contact waste package surfaces over the thermal history of the repository as it heats up and cools back down to ambient conditions. In the above-boiling period, brines will be characterized by high nitrate to chloride ratios that are stable to higher temperatures than previously predicted. This is clearly shown for the NaCl-KNO_3 salt system in the deliquescence and boiling point experiments in this report. Our results show that additional thermodynamic data are needed in nitrate systems to accurately predict brine stability and composition due to salt deliquescence in dust deposited on waste package surfaces. Current YMP models capture dry-out conditions but not composition for NaCl-KNO_3 brines, and they fail to predict dry-out conditions for NaCl-KNO_3-$NaNO_3$ brines. Boiling point and deliquescence experiments are needed in NaCl-KNO_3-$NaNO_3$ and NaCl-KNO_3-$NaNO_3$-$Ca(NO_3)_2$ systems to directly determine dry-out conditions and composition, because these salt mixtures are also predicted to control brine composition in the above-boiling period. Corrosion experiments are needed in high temperature and high NO_3:Cl brines to determine if nitrate inhibits corrosion in these concentrated brines at temperatures above 160°C.

Chemical transformations appear to be important for pure calcium- and magnesium-chloride brines at temperatures greater than 120°C. This stems from a lack of acid gas volatility in NaCl/KNO_3 based brines and by slow CO_2(g) diffusion in alkaline brines. This suggests that YMP corrosion models based on bulk solution experiments over the appropriate composition, temperature, and relative humidity range can be used to predict corrosion in thin brine films formed by salt deliquescence.

In contrast to the above-boiling period, the below-boiling period is characterized predominately by NaCl based brines with minor amounts of K, NO_3, Ca, Mg, F, and Br at less than 70% relative humidity. These brines are identified as sulfate and bicarbonate brines by the chemical divide theory. Nitrate to chloride ratios are strongly tied to relative humidity and halite solubility. Once the relative humidity is low enough to produce brines saturated with respect to halite, then NO_3:Cl increases to levels and may inhibit corrosion. In addition to the more abundant NaCl-based brines some measured pore waters will evaporate towards acid NaCl-$CaCl_2$ brines. Acid volatility also occurs with this brine type indicating that chemical transformations may be important in thin

[1] Corresponding Author
email: carroll6@llnl.gov

films. In contrast to the above-boiling period, comparison of our experimental data with calculated data suggest that current YMP geochemical models adequately predict in-drift chemistry in the below-boiling period.

1.0 Introduction

The in-drift chemical environments at waste package surfaces will be characterized by the evaporation of seepage pore water and by the deliquescence of salts found in deposited dusts. Brine chemistry will be highly dependent on the evolving temperature and relative humidity as the repository initially heats up and cools back down to ambient conditions. We can breakdown the in-drift environments to an above boiling period in which high temperatures prevent seepage pore water from dripping onto the waste package surfaces. In this time period (about 1000 years) brines form by the deliquescence of salts found in dust deposited on the waste package surfaces during construction and ventilation of the repository. In the below-boiling period (about 1000 to 100,000 years), brines form by both the evaporation of pore water dripping onto the waste package surfaces (assuming no drip shield) and by the deliquescence of salts in deposited dust.

The focus of LLNL's environmental sciences technical area for the Yucca Mountain Project is to conduct experiments that simulate brine chemistry likely to contact the waste package surfaces over the thermal and relative humidity history of the repository. These experiments provide direct empirical information on chemical environments that may react with the waste package surfaces. They also comprise a validation data set that can be used to determine the uncertainty between model calculations of the chemical environments over wide thermal and relative humidity history of the repository. This is important, because calculation of brine chemistry relies on the YMP Pitzer Model to account for non-ideal behavior of concentrated multi-component solutions.

In this report, we summarize mixed salt deliquescence, boiling point, and resistivity experiments designed to determine brine chemistry in the above-boiling period. We summarize thin film chemical transformation experiments designed to determine the stability of likely brines in the above-boiling period. We also summarize the evaporation of three pore water types to determine the chemical controls of brine formation in the below-boiling period.

2.0 Deliquescence of NaCl-KNO_3 salt mixtures at 90 and 120˚C

We studied the brine chemistry in the NaCl-KNO_3-H_2O system because halite and niter are predicted to be the dominant salt mixtures in dusts at waste package surfaces (BSC 2004a). Accurate prediction of brine formation is important for the safe disposal of radioactive waste, because brine composition is an indicator of the corrosiveness of the aqueous environment and the relationship between deliquescence relative humidity and temperature is an indicator of "repository dryness". Deliquescence refers to the formation of an aqueous solution by the absorption of water by hygroscopic salt minerals. This process allows brines to form above 100˚C at atmospheric pressure. The relative humidity at which salts deliquesce is dependent on temperature and is characteristic to each salt mineral or assemblage of salt minerals.

We compare model predictions and experimental results of relative humidity and solution compositions in saturated NaCl-KNO_3-H_2O system at 90 and 120ºC (experimental data are in DTN: LL040200623121.037 and LL040311523121.039). More detailed description of these results, as well as the deliquescence chemistry of NaCl-$NaNO_3$-H_2O and KNO_3-$NaNO_3$-H_2O systems can be found in Carroll et al. (2005). All geochemical modeling uses EQ3/6 code and the YMP Pitzer data base (BSC 2004b).

2.1 Methods

We measured brine composition at controlled relative humidity for NaCl-KNO_3 salt mixtures from 90 to 120˚C as a function of X_{Na}. We approached the equilibrium brine composition by placing identical mole fractions of dissolved and solid salt mixtures in an environmental chamber (Ecosphere, Despatch) at controlled relative humidity and temperature. Under these conditions the dissolved salt mixture evaporates concentrating the solution and precipitating one of the two salts, and the solid salt mixture absorbs water dissolving the salts until equilibrium is reached. Calibrated temperature and relative humidity probes were place just above the solutions in the beakers, because microenvironments within the beakers differed from the environmental chamber relative humidity by as much as 5% relative humidity. Relative humidity probe calibration checks were conducted in saturated KNO_3 solutions from 90 to 110˚C. Statistical analysis of these RH measurements together with vapor pressure measurements for KNO_3 (Kracek, 1928) yields an average standard deviation of about 1.6 RH units. Uncertainty reported in the tables and figures is calculated as 2s or 3.1 RH units. About one gram of solution was collected from each beaker and filtered through a 0.45m syringe-less filter into a sampling bottle, the bottle was sealed and weighed to determine sample amount, and then diluted with about 250 grams of distilled and deionized water. All dilution factors were determined gravimetrically. Solution composition was determined from ion chromatograph or inductively coupled plasma-atomic emission analysis of diluted solutions. Solids were separated from the remaining solution by filtration (0.45m pore size), dried, and stored in desiccators until analyzed by powder X-ray diffraction. All model calculation were made with the current high-temperature Pitzer model (BSC 2004b)

2.2 Comparison of model and experimental results

Figures 1 and 2 compare the experimental results of the reversed deliquescence experiments with the model calculations for the NaCl-KNO_3-H_2O system at 90˚C and 120˚C. The convergence between the measured relative humidity and solution composition for initially dissolved and initially solid salt mixtures indicates that equilibrium was achieved. Values for the deliquescence relative humidity are in agreement at both temperatures. This agreement at the eutectic relative humidity appears to be fortuitous, because there is poor agreement between experiment and model for most other relative humidity values and all solution compositions. The extent of the mismatch is much greater at 120˚C than at 90˚C. At 90˚C, the greatest mismatch occurs in KNO_3-rich solutions where the model under predicts relative humidity by as much as five percentage points and under predicts solution composition by as much as 4 molal (about 30%). In solutions dominated by NaCl (X_{Na}>0.5), there is reasonable agreement between model and experiment. At 120˚C, the mismatch between experiment and model

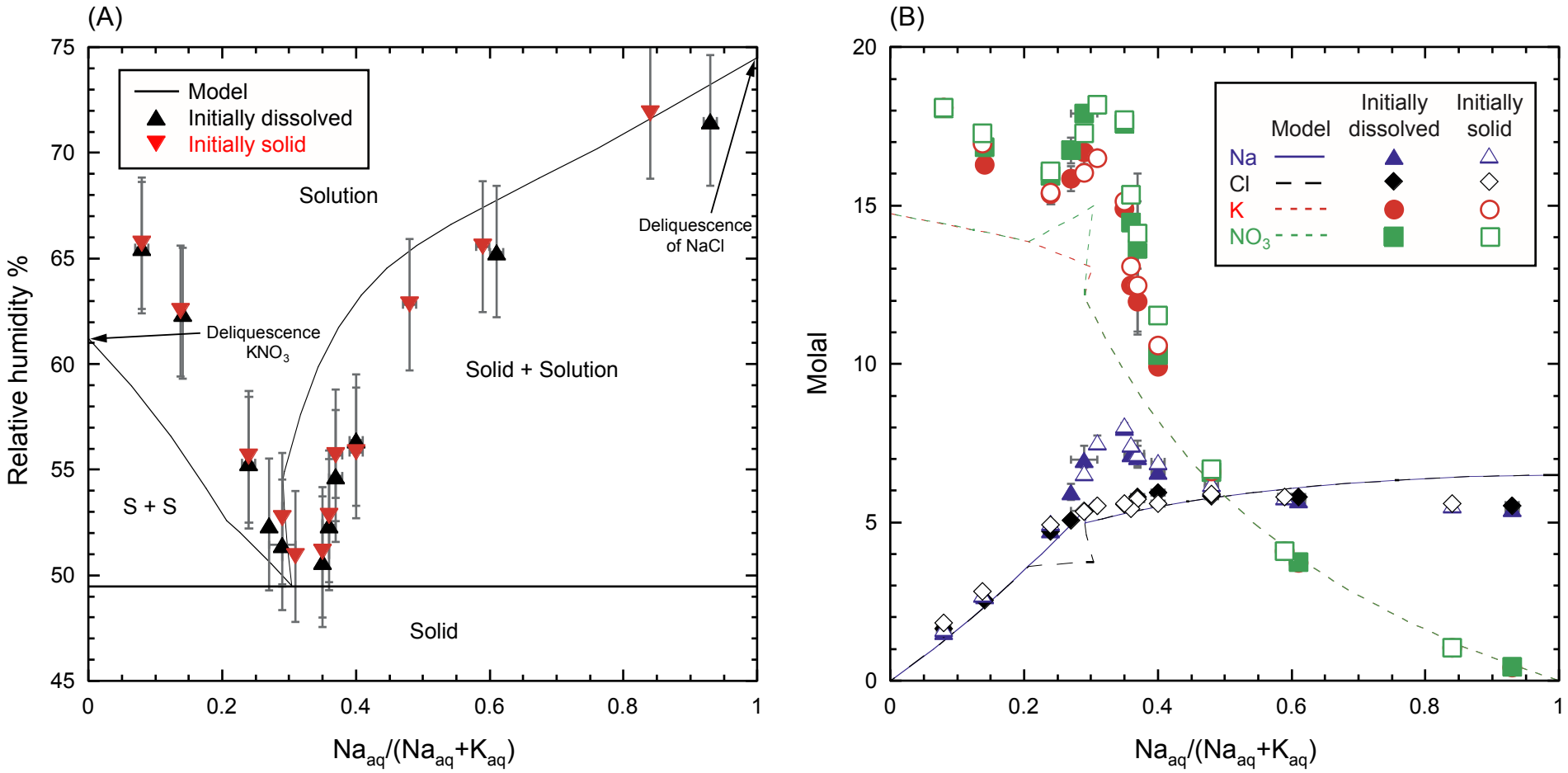

Figure 1. Deliquescence of NaCl-KNO_3 salts at 90ºC starting from initially dissolved and initially solid mixtures plotted as (A) % relative humidity and (B) solution composition.

$NaCl\text{-}KNO_3\text{-}H_2O$ at 120°C

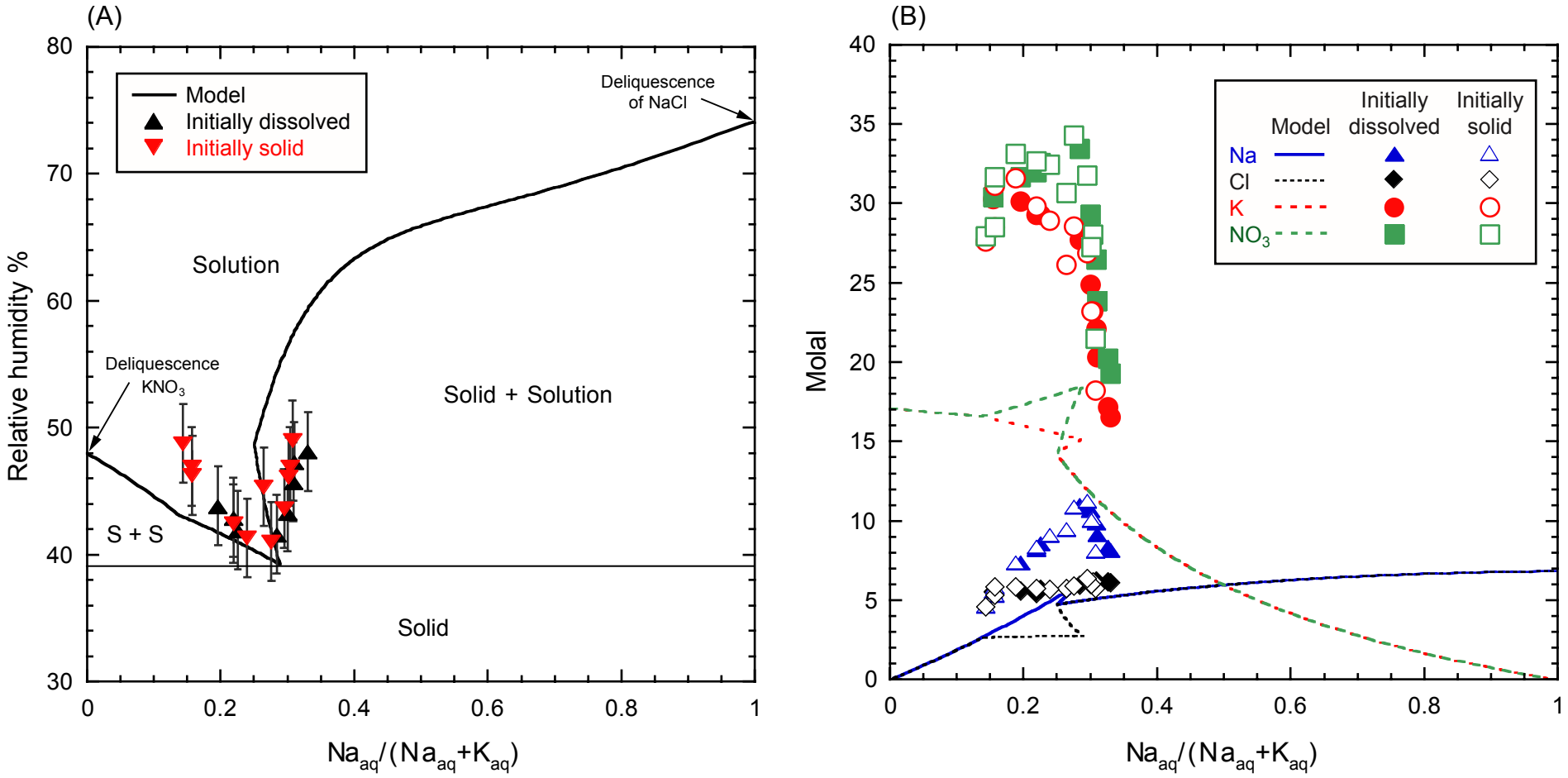

Figure 2. Deliquescence of $NaCl\text{-}KNO_3$ salts at 120°C starting from initially dissolved and initially solid mixtures plotted as (A) % relative humidity and (B) solution composition.

relative humidity is similar to that at 90˚C. However, at this higher temperature, the model significantly under predicts the solution composition. In the most extreme case, solution compositions are roughly twice the model prediction with experimental sodium = 11 molal, potassium = 28 molal, chloride = 6 molal, and nitrate = 33 molal. Analysis of the solids shows that sylvite is an important solubility control near the experimental eutectic. At 90˚C, niter, sylvite and minor amounts of halite were detected just to the left of the eutectic ($0.28 \leq X_{Na} \leq 0.31$), and halite, sylvite and minor amounts of niter were detected to the right side of the eutectic ($0.35 \leq X_{Na} \leq 0.40$). As is expected, the solids consisted of niter ($X_{Na} \leq 0.25$) and halite ($X_{Na} \geq 0.60$) on their respective limbs of the phase diagram. At 120˚C, solutions were saturated with respect to niter, sylvite, and halite for most of the samples between $0.15 \leq X_{Na} \geq 0.30$. Any trace amounts of salt detected probably represent residual solution that was trapped in pore spaces during the filtration process when the salts were dried.

The comparison of model predictions and experimental results of relative humidity and solution compositions for the $NaCl\text{-}KNO_3\text{-}H_2O$ systems at 90ºC and 120ºC indicate that some parameters used in the current high-temperature Pitzer model do not adequately describe brine chemistry formed by deliquescence. The Yucca Mountain Project Pitzer model contains temperature dependent sub models for the $Na\text{-}NO_3$, Na-Cl, K-Cl, Na-K, and K-Na-Cl ion interactions (Archer 2000; Rard and Wijesinghe, 2003; Pitzer et al., 1984; Møller 1988, Holmes et al, 1978; Holmes and Mesmer, 1983). However, the $K\text{-}NO_3$ and $Cl\text{-}NO_3$ sub models are based on only 25˚C data (Pitzer 1991) and there are no parameters for the $Na\text{-}K\text{-}NO_3$, $Na\text{-}Cl\text{-}NO_3$, or $K\text{-}Cl\text{-}NO_3$ ion interactions. The absence of temperature dependent parameters for $K\text{-}NO_3$ ion interactions in the Yucca Mountain Project Pitzer model is the primary cause of the poor prediction of the deliquescence of salt mixtures containing KNO_3 at elevated temperatures (Figures 1-2) as well as the measured % relative humidity and solubility of KNO_3 at elevated temperature (Figure 3). Additionally, some of the mismatch in the $NaCl\text{-}KNO_3\text{-}H_2O$ may also be due to the absence of temperature dependent parameters for $Cl\text{-}NO_3$, $Na\text{-}Cl\text{-}NO_3$, and/or $K\text{-}Cl\text{-}NO_3$ ion interactions.

2.3 Implications for localized corrosion model

Our experimental results show that dry-out temperatures for the $NaCl\text{-}KNO_3\text{-}H_2O$ system are fairly well predicted by the model, indicating that predictions for this system can be used to indicate temperature and relative humidity range where brines will exist at the waste package surface. The significant under prediction of the dissolved nitrate concentrations at high temperatures results in a conservative estimation of localized corrosion, because nitrate reduces the initiation of localized corrosion in the current model (BSC 2004c).

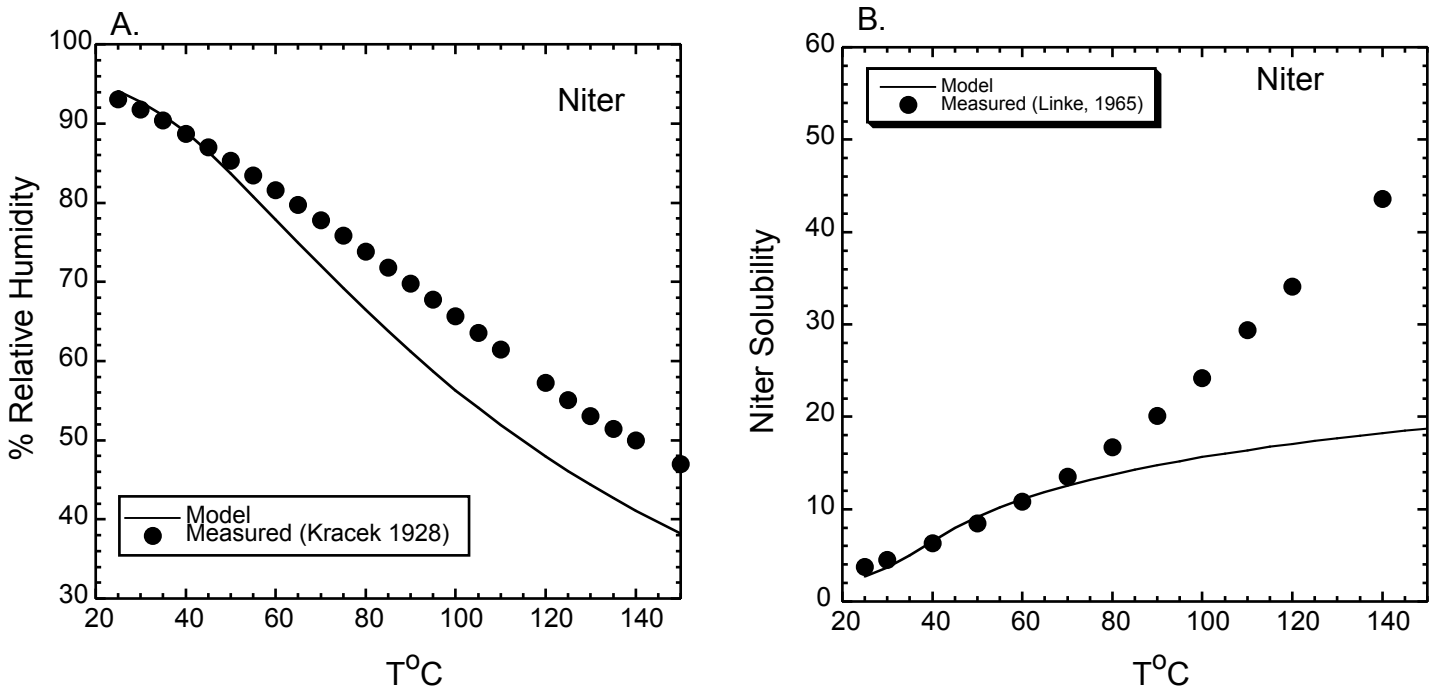

Figure 3. Comparison of predicted and measured niter (KNO_3) (A) % relative humidity and (B) solubility as a function of temperature. Predictions were made using EQ3/6 version 8 geochemical code and the Yucca Mountain high temperatured Pitzer ion interaction thermodynamic data base (BSC 2004a,b).

3.0 Boiling Temperature Measurements for Saturated Solutions in the Systems $NaCl-KNO_3-H_2O$, $NaNO_3-KNO_3-H_2O$, and $NaCl-NaNO_3-KNO_3-H_2O$

Boiling temperature measurements were made to directly establish the upper temperatures at which deliquescence can occur in the following salt systems: $NaCl-KNO_3-H_2O$, $NaNO_3-KNO_3-H_2O$, and $NaCl-NaNO_3-KNO_3-H_2O$. The $NaCl-KNO_3-H_2O$ and $NaCl-NaNO_3-KNO_3-H_2O$ salt systems were studied, because they are predicted to be the two most dominant brines formed by the deliquescence of salts in dusts at the waste package surface (BSC 2004a). It is important to make these measurements because the temperature-dependent $K-NO_3$ and $Cl-NO_3$ solution Pitzer parameters needed for improving the thermodynamic modeling predictions are not likely to be available in the near future. These measurements will also provide checks on the reliability of future geochemical modeling calculations. Details of the methods and results are available in Rard (2004) and the data are in DTN: LL040901831032.008.

3.1 *Methods*

Most of the boiling point measurements were made in 1-liter glass apparatus fitted with a water-cooled condenser column to reduce loss of water during the experiments. The bottom section of the apparatus was inserted into a heating mantle, with heat being applied separately to the bottom and to the sides of the apparatus. Salt solutions were stirred and temperature was measured at two different depths to check for adequate mixing. The basis experimental procedure is as follows. About 100 to 150 ml of purified water was added to the boiling temperature apparatus and the heaters in the heating mantle were turned on to begin the heating process. Known weights of solid salt were transferred to the boiling temperature apparatus through an open port to yield a saturated solution together with an excess of solid phase. Heating was continued until the solution began boiling, and the boiling temperature of the saturated solution was recorded. A sample of a second salt was then weighed and transferred to the boiling temperature apparatus to produce a mixed salt system containing excess solid salt, and the boiling temperature of this mixture was determined in the same manner. Generally, additional amounts of the second salt were added in stages, and the saturated solution boiling temperatures were measured for these additional mixture compositions. The boiling temperatures of the saturated solutions in the mixed salt systems were always significantly higher than those of the corresponding single salt systems, and sometimes this temperature increase was sufficient to cause all of the solid salts that had been added to dissolve. When this happened, an additional amount of the first salt was added to yield another saturated solution.

3.2 Boiling Temperatures for the $NaCl-KNO_3-H_2O$ System

The corrected boiling temperatures for saturated solutions in the $NaCl-KNO_3-H_2O$ system are plotted in Figure 4 as a function x_{NaCl} solid added to the solution. At the observed eutectic composition, which corresponds to the maximum boiling temperature, the solution composition fractions should be the same as their nominal values of solid mixture. Our boiling temperatures are consistent with the eutectic composition occurring at $x(NaCl) \approx 0.32$, $x(KNO_3) \approx 0.68$, and a maximum boiling temperature of 133.8°C at 0.99 bar. The boiling temperature agrees well with predicted dry-out temperature of 130°C at 0.98 bar for the $NaCl + KNO_3 + H_2O$ system (BSC 2004a) using the YMP

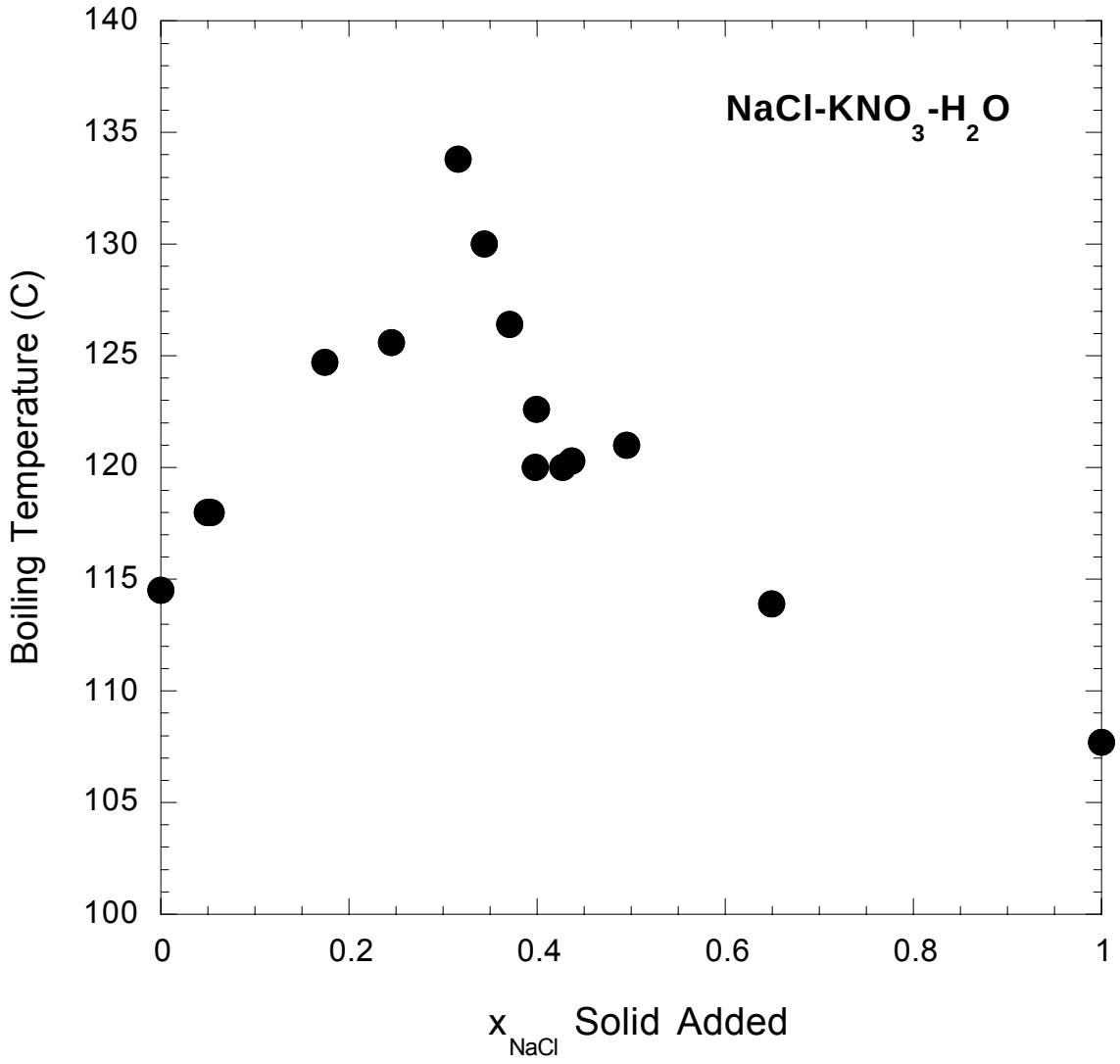

Figure 4. Boiling points measured in the NaCl-KNO_3-H_2O system in saturated solutions as a function of the x_{NaCl} solid added to the solution.(BSC 2004b).

Pitzer model. These values are also consistent with trends in experimental deliquescence relative humidity for this salt mixture (Carroll et al., 2005).

3.3 Boiling Temperatures for the $NaNO_3$-KNO_3- H_2O System

The corrected boiling temperatures for saturated solutions in the $NaNO_3$-KNO_3-H_2O system are plotted in Figure 5 as function of the x_{NaNO3} solid added to the solution. A maximum is observed in the boiling temperatures around 160°C with a composition fraction of $x(NaNO_3) \approx 0.46$ and $x(KNO_3) \approx 0.54$, which should correspond to the eutectic composition. This maximum boiling temperature is ≈ 40°C above that observed for the limiting binary solution $NaNO_3 + H_2O$ and ≈ 52°C above that observed for the other limiting binary solution $KNO_3 + H_2O$. Available solubility for the $NaNO_3 + KNO_3 + H_2O$ system yield eutectic compositions of $x(NaNO_3) = 0.391$ at 125 °C, $x(NaNO_3) = 0.425$ at

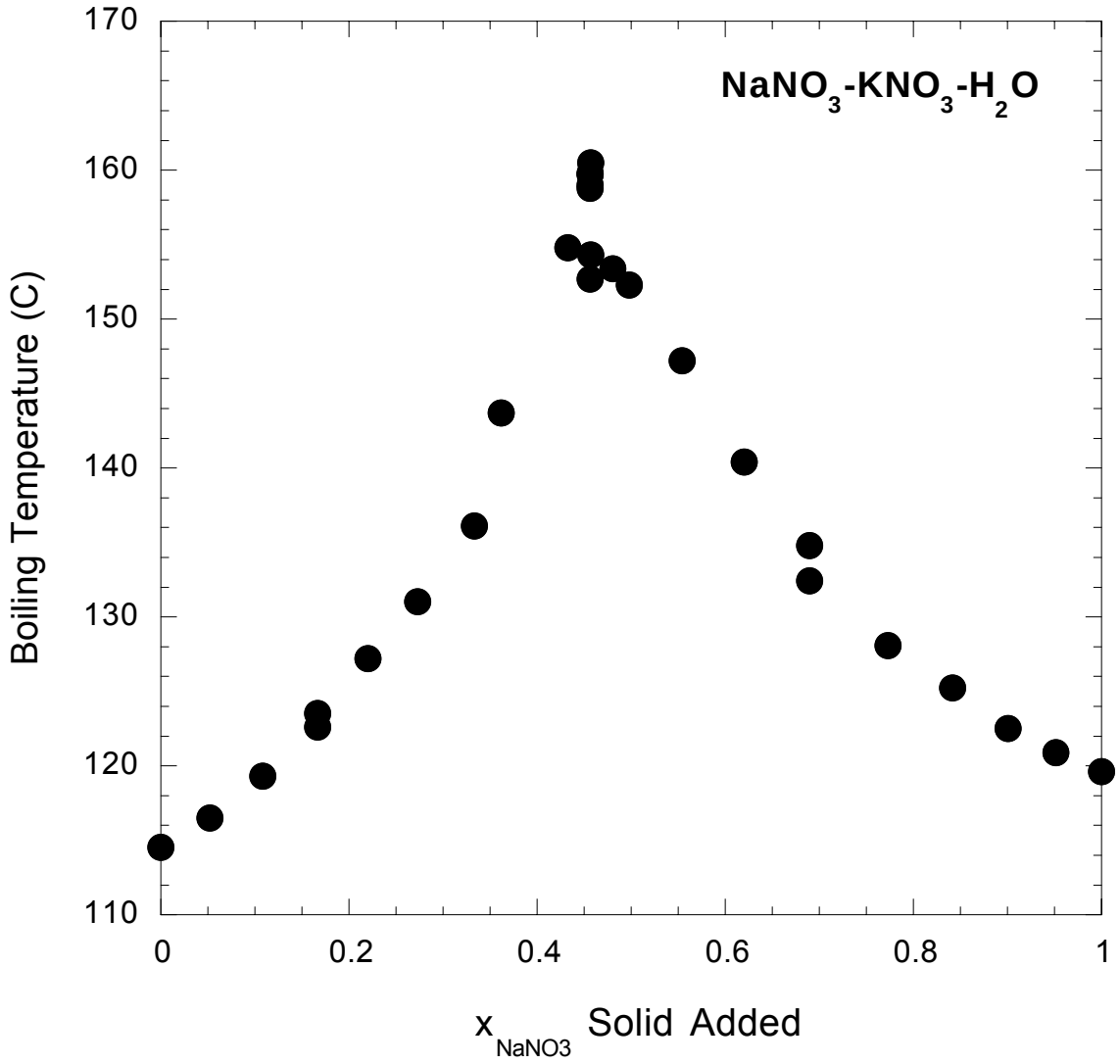

Figure 5: Boiling points measured in the $NaNO_3$-KNO_3-H_2O system in saturated solutions as a function of the x_{NaNO3} solid added to the solution.

150°C, and x($NaNO_3$) = 0.467 at 175°C, which are consistent with our result at the maximum boiling temperature of ≈ 160°C (Linke, 1965).

3.4 Boiling Temperatures for the NaCl-$NaNO_3$-KNO_3-H_2O System

The corrected boiling temperatures for saturated solutions in the NaCl-$NaNO_3$-KNO_3-H_2O system are plotted in Figure 6 as a function of the x_{NsCl} solid added to the solution at two specific mole ratios of KNO_3:$NaNO_3$ of 1.01 and 1.19. A KNO_3:$NaNO_3$ = 1.19 corresponds to the eutectic ratio of the $NaNO_3$-KNO_3-H_2O system. Addition of NaCl resulted in a large increase in the observed boiling temperatures, with the highest observed boiling temperature being 195.7 °C. It is likely that the eutectic boiling temperatures will

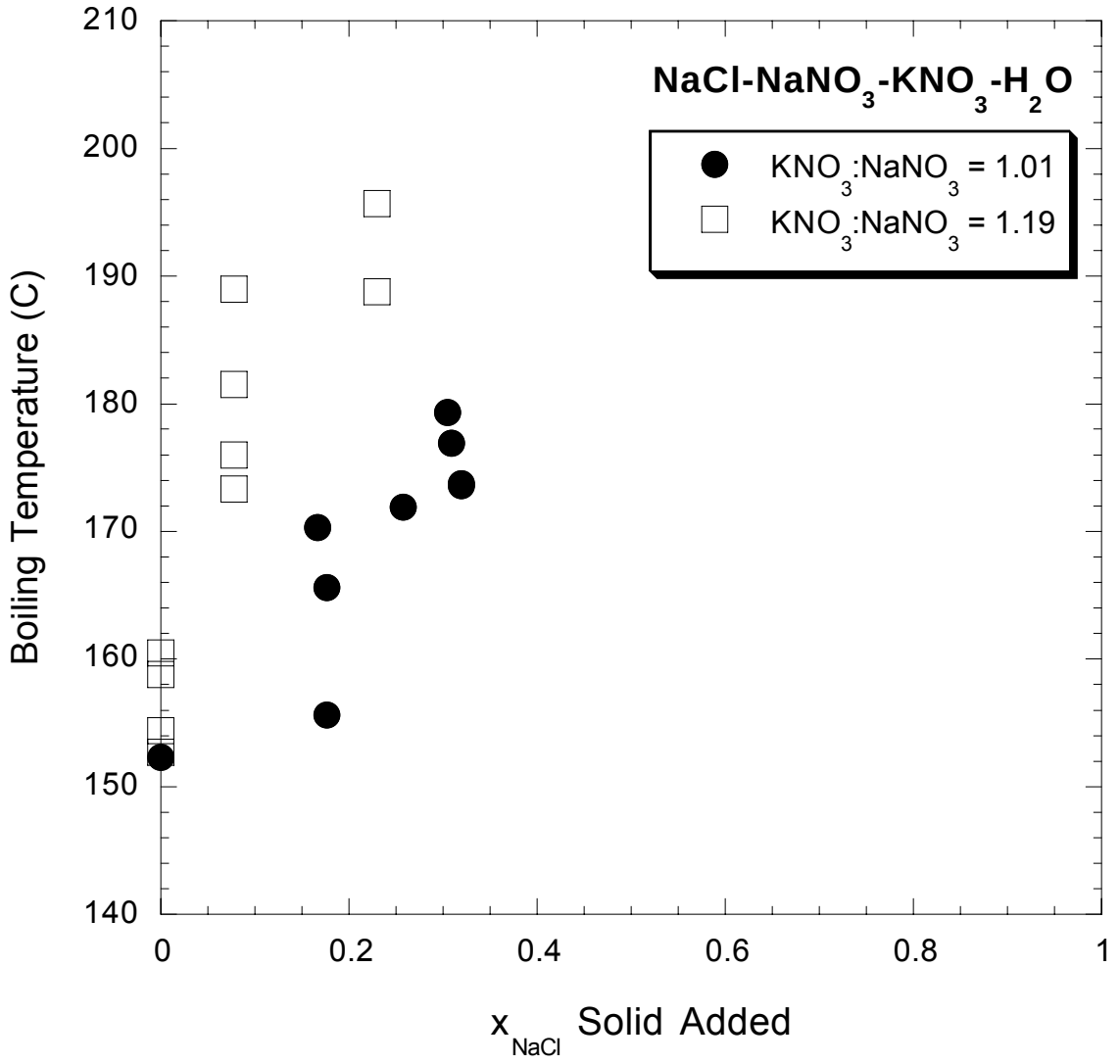

Figure 6: Boiling points measured in the NaCl-$NaNO_3$-KNO_3-H_2O system in saturated solutions as a function of the x_{NsCl} solid added to the solution at two specific mole ratios of KNO_3:$NaNO_3$ of 1.01 and 1.19. A KNO_3:$NaNO_3$ = 1.19 corresponds to the eutectic ratio of the $NaNO_3$-KNO_3-H_2O system.

exceed 200°C, because the observed boiling temperatures continued to increase with increasing values of x(NaCl), both when KNO_3:$NaNO_3$ ≈ 1.01 and when KNO_3:$NaNO_3$ ≈ 1.19. In contrast to the NaCl-KNO_3-H_2O system in which model predictions of the dry-out temperatures were in good agreement with experimental results, in the NaCl-$NaNO_3$-KNO_3-H_2O system dry-out temperatures are nearly 60°C lower than the measured boiling points (BSC 2004ab).

3.5 *Implications for localized corrosion at elevated temperatures*

Our experimental results show that dry-out temperatures for the NaCl-KNO_3-H_2O system are fairly well predicted by the model, indicating that predictions for this system can be used to indicate temperature and relative humidity ranges where these brines are stable in the in-drift environment. This is not the case for the NaCl-$NaNO_3$-KNO_3-H_2O system, where the experimental results indicate some dust samples from the Yucca Mountain Site will deliquesce at temperatures ≥ 196 °C. The current abstraction model for localized corrosion initiates localized corrosion for all water films in contact with the waste package surfaces at temperatures above 160°C (BSC 2004c). This may be too conservative for Alloy 22 because the high nitrate solutions in the NaCl-$NaNO_3$-KNO_3-brines may inhibit localized corrosion even at these higher temperatures.

4.0 Deliquescence of Na-K-Cl-NO_3 salt mixtures up to 180˚C using resistivity techniques

Resistivity experiments were conducted as a function of relative humidity in an effort to directly measure the deliquescence relative humidity for the NaCl-KNO_3-$NaNO_3$-H_2O salt system at high temperatures (140 to 180˚C) to confirm the elevated boiling points measured for the salt system (see section 3.0 and Rard, 2004). We also studied the deliquescence of NaCl at 105˚C, NaCl-KNO_3 at 120˚C and KNO_3-$NaNO_3$ at 140 and 180˚C. The basic premise behind the resistivity experiments is that the resistance will significantly drop at the DRH for a given salt mixture as the brine solution forms. This approach as also been used to measure the DRH of pure salts and NaCl-KNO_3 salt mixtures to 86˚C (Yang et al, 2002). It is important to confirm the boiling point measurements with an independent set of experiments, because the current TSPA model initiates localized corrosion of Alloy 22 for all solutions above 160˚C (BSC 2004c). Details of the methods and results are available in Carroll et al (2004) and the data are in DTN: LL041001423121.046.

4.1 Methods

We measured the deliquescence NaCl-KNO_3, KNO_3-$NaNO_3$, and NaCl-KNO_3-$NaNO_3$ salts from 105 to 180˚C by varying the relative humidity and monitoring the resistivity of the salt systems. All experiments were conducted in environmental chambers to control temperature and relative humidity. Temperature was limited to the maximum of 180˚C to prevent deterioration of the relative humidity probe. Relative humidity was limited to the maximum achievable relative humidity at atmospheric pressures. Relative humidity measurements made below 120˚C are accurate to ±1.6 %RH (Carroll et al., 2005). All relative humidity values made above 120˚C are conditional values because the lower temperature calibration was not checked.

The resistivity experiments consisted of two parallel platinum electrodes spaced less than one millimeter apart across a recessed reaction cell made of PVDF (polyvinylidene fluoride; good to 150˚C) or PPS (polyphenylene sulfide; good above 180˚C), where the length of the electrodes exposed to the solution was about to 2.5cm. A second design contained the same electrode spacing but a quartz slide was placed directly under the electrodes to provide an inert surface. Experiments conducted with and without the glass slide showed no difference, suggesting that the PVDF and PPS materials were also inert to brine chemistry and no sorption of water at low relative humidity and high temperature by the reaction cell. Resistance was monitored by an automated data

acquisition system with a Gamry PCI4/300 Potentiostat in which one Pt-electrode was the working electrode and the other was the counter and reference electrode. All measurements were recorded in electrochemical impedance spectroscopy (EIS) mode at 5000 hertz where the voltage reference and the direct current voltage bias were set to zero, with an alternating current voltage of 20 or 25mv. Temperature and relative humidity inside the environmental chamber were measured just above the cells. All experiments started enough dissolved salt to provide a conductive path between the electrodes (about 80% coverage). Cells were cleaned and the impedance checked before each new solution was added.

4.2 NaCl-KNO_3 at 120˚C

We measured the deliquescence of NaCl-KNO_3 at 120˚C and 1 bar to verify that the resistivity techniques could measure the deliquescence of salt mixtures. We observe deliquescence of NaCl-KNO_3 between 37% and 41%RH with a total drop in impedance of 4 to 5 orders of magnitude (Figure 7). These RH values are consistent with experimental DRH determined form solubility experiments for NaCl-KNO_3 of 39% RH at 120˚C (Carroll et al., 2005). The step-wise decrease in impedance over each RH increment may indicate the absorption of monolayers of water at 37% RH followed by macroscopic deliquescence at slightly higher RH. Decreasing RH between increments also suggests equilibrium was not reached over 2 hour time steps even for thin salt films.

4.3 NaCl-KNO_3-$NaNO_3$ and -KNO_3-$NaNO_3$ from 140˚C to 180˚C

NaCl-KNO_3-$NaNO_3$ salt mixtures are calculated to represent about 30% of the deliquescent salt assemblages present in dusts that may contact the repository (BSC, 2004a). Our resistivity experimental results support elevated boiling points of 196˚C reported by Rard (2004). Figure 8 shows a two to three decade drop in impedance for NaCl-KNO_3-$NaNO_3$ salt mixtures at conditional RH of 22% at 140˚C and 12 to 14% at 180˚C indicating the presence of a brine solution at temperatures much higher than the predicted dry-out temperatures of about 140˚C at 1 bar (136˚C at 0.9 bar, BSC 2004a). The drop in impedance clearly shows the absorption of water vapor by the salt assemblage above the predicted dry-out temperature. As expected we see a decrease in deliquescence relative humidity with increasing temperature. The absence of deliquescence at 170˚C probably indicates that the experiment was stopped prior to achieving the deliquescence relative humidity.

We conducted KNO_3-$NaNO_3$ deliquescence experiments together with the NaCl-KNO_3-$NaNO_3$ deliquescence experiments as an intended control. The KNO_3-$NaNO_3$ salt mixture should not deliquescence above its boiling point of 160˚C (Rard 2004). However our experiments clearly show that KNO_3-$NaNO_3$ salt mixtures absorb water at 180˚C and as expected at 140˚C(Figure 9). It is possible that the observed one to two decade drop in impedance at 180˚C reflects absorption of monolayers of water rather than full thermodynamic deliquescence observed in boiling point and solubility experiments (Carroll et al., 2004a). This explanation is consistent with observed absorption of water at relative humidity lower than the equilibrium deliquescence in similar salt mixtures (Ge et al, 1998; Yang et al, 2002). At this time we cannot correlate the absolute impedance drop with brine volume, because it may also reflect changes in temperature and solution composition as well as the extent of electrode wetness.

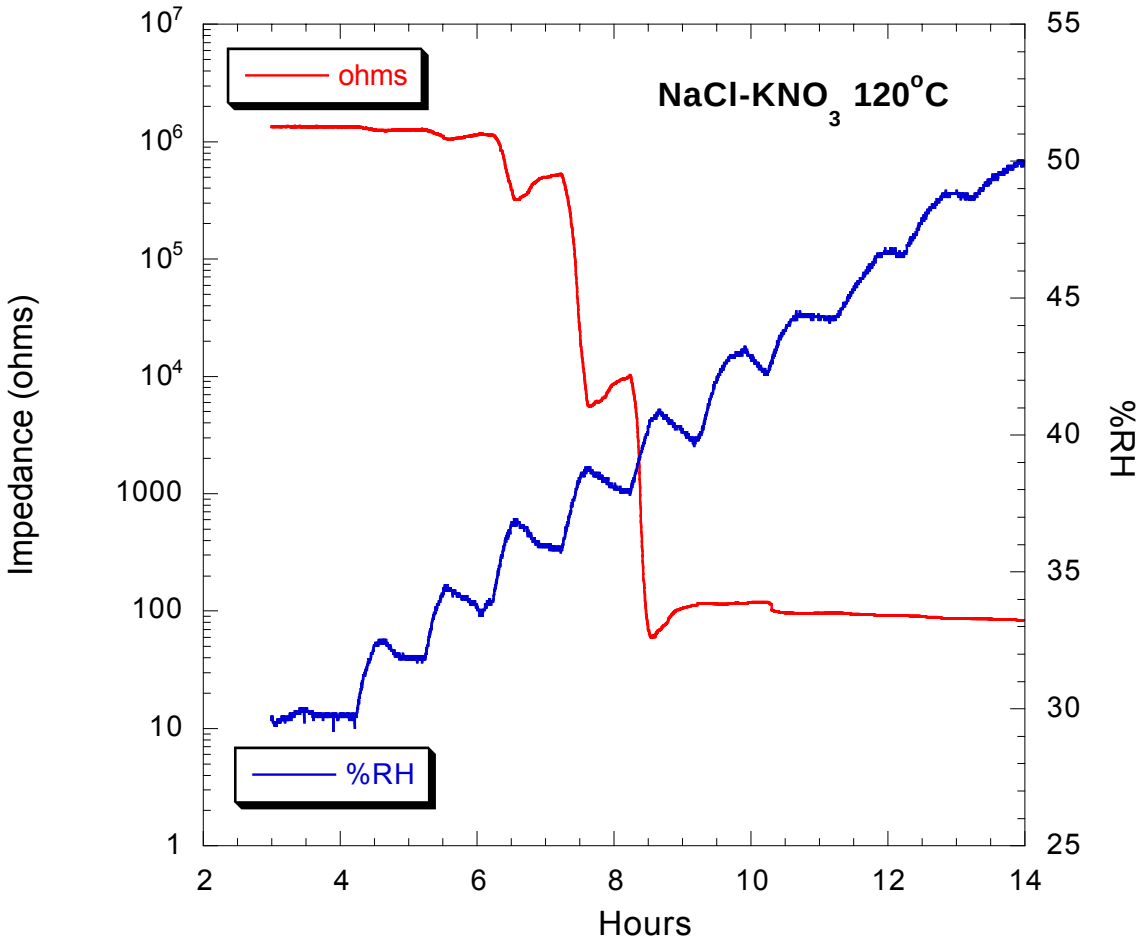

Figure 7. Deliquescence of NaCl-KNO_3 salt mixtures at 120˚C and 1 bar shown as log impedance and %RH vs. time. Experimental data can be found in DTN-LL041001423121.046

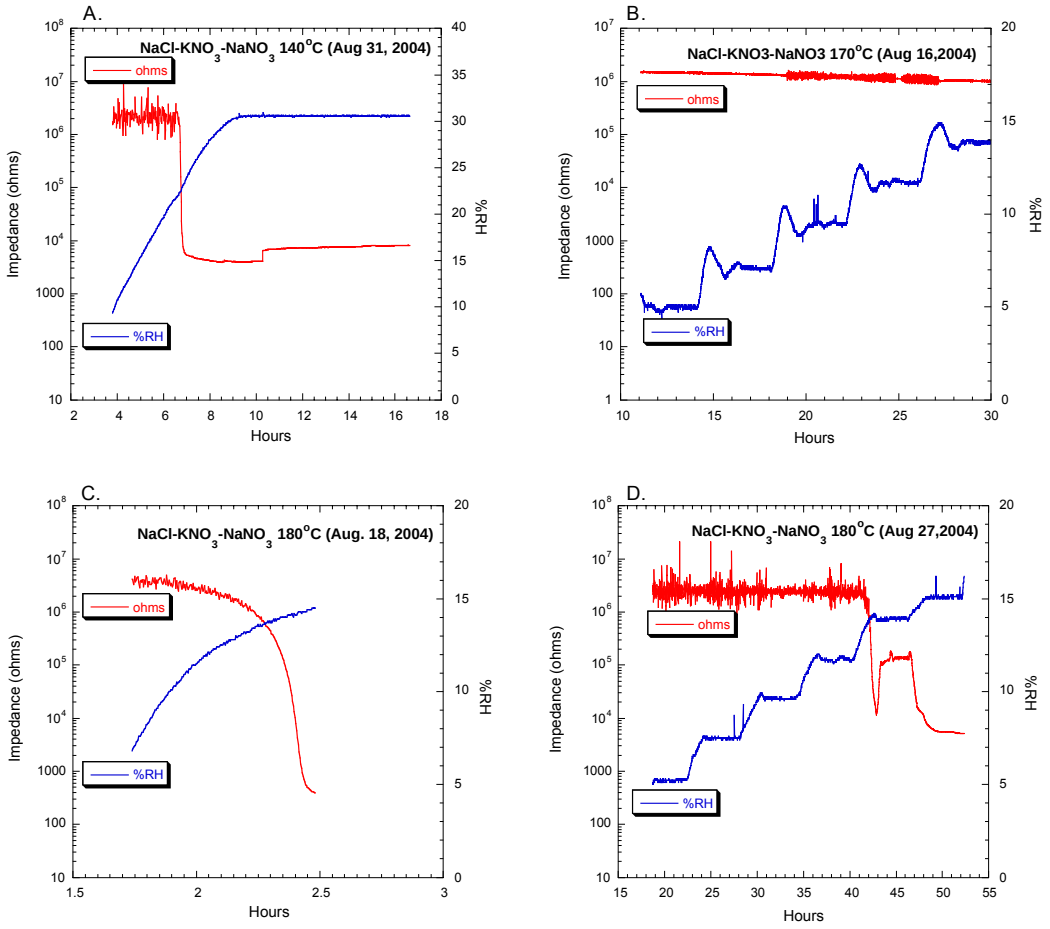

Figure 8. Deliquescence of KNO_3-$NaNO_3$ salt mixtures at 140, 170, and 180˚C and 1 bar shown as log impedance and %RH vs. time. Experimental data can be found in DTN-LL041001423121.046

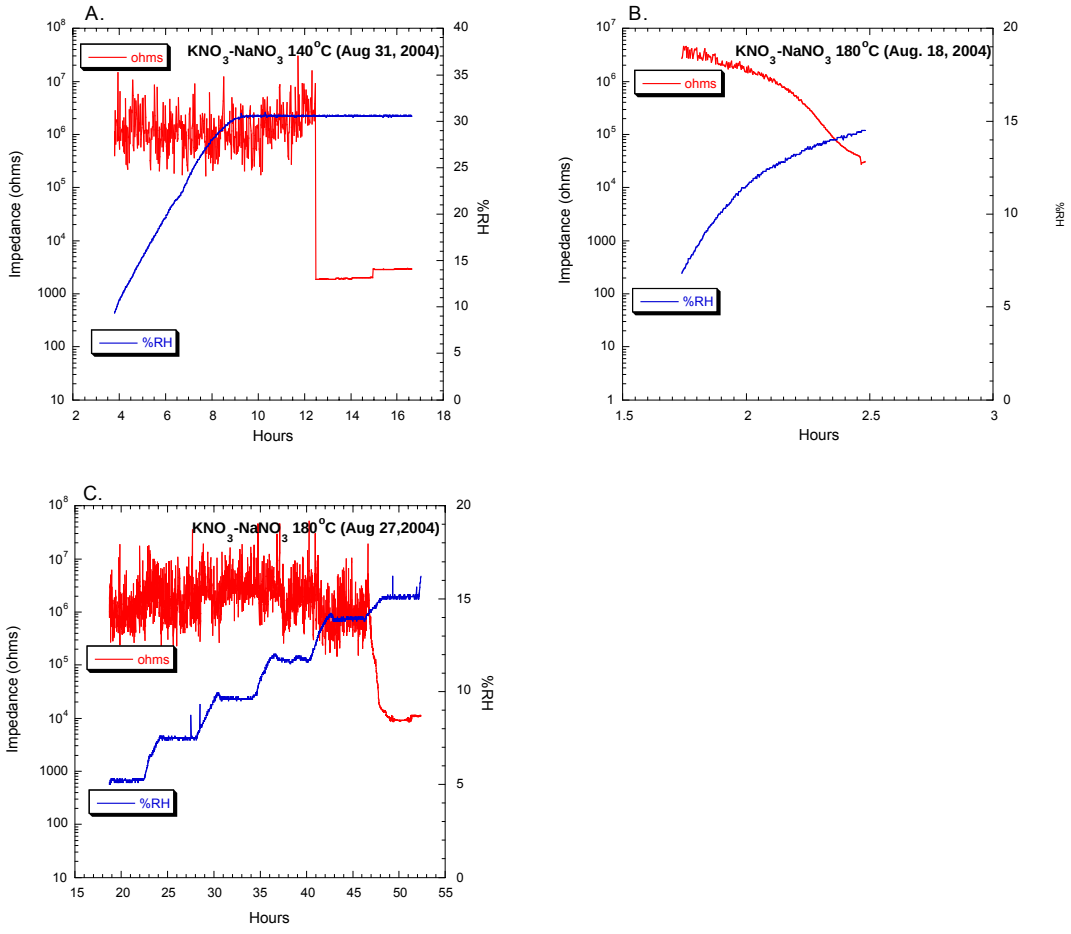

Figure 9. Deliquescence of KNO_3-$NaNO_3$ salt mixtures at 140, 170, and 180˚C and 1 bar shown as log impedance and %RH vs. time. Experimental data can be found in DTN-LL041001423121.046

4.4 Implications for localized corrosion at elevated temperatures

Comparison of our results to dry-out temperatures predicted with the current Yucca Mountain Pitzer model (BSC 2004a) and recent boiling point measurements (Rard 2004) show that model predictions for NaCl-KNO_3 brines agree with experiment, however model calculations significantly under predict dry-out of NaCl-KNO_3-$NaNO_3$ brines. This implies that brines can form in a repository environment at much higher temperatures and lower relative humidity. YMP Waste package corrosion models need to be based on experiments that span temperature, relative humidity and corresponding solution composition of brines formed from these deliquescent salt mixtures. Our results also show that water absorbs to KNO_3-$NaNO_3$ at 180˚C, well above its boiling point of 160˚C. This may represent absorption of monolayers of water at the salt surface.

5.0 Chemical Transformations in thin films on Alloy 22

Understanding the effect of thin film chemistry on Alloy 22 corrosion is important for the Yucca Mountain Project, because brines formed by the deliquescence of salts present in dusts on waste package surfaces in the above-boiling period will be present as thin films and not bulk solutions. Current corrosion YMP models are based on experimental data from bulk solutions. Although the underlying mechanisms for electrochemical corrosion, such as the oxidation of iron at the anode and reduction of oxygen at the cathode are identical for both bulk solution and thin film corrosion, the very nature of the thin film can result in chemical transformations that alter the chemistry of the thin film and the extent of corrosion. Features that contribute to chemical transformations in aqueous thin films are gas diffusion within the thin film, and solid precipitation at cathodic and anodic sites.

At high temperatures expected in the in-drift environment, gas volatility may drive chemical transformations in thin films by altering the brine chemistry. Thin film acidity may be inherent to the thin film chemistry or a product of metal ion hydrolysis from corrosion. Generally the partial pressure of acid gases increases with increasing temperature and with decreasing pH. In an open system like the in-drift environment, any acid gases will be transported out of the thin film, causing pH to increase. At higher pH, atmospheric carbon dioxide (CO_2) should diffuse into the thin film. Higher pH and dissolved carbonate thermodynamically favors the precipitation of hydroxide and carbonate minerals. These solids are insoluble relative to the initial deliquescence of salts, and would result in the evaporation of water. Corrosion would then cease in the absence of a conducting fluid.

Chemical transformations can be further enhanced by electrochemical processes because transport limited diffusion may allow the build up of hydroxyl ions at the cathode. Under the oxidizing conditions expected in the in-drift environment, oxygen reduction is the dominant reaction at the cathode:

$$0.5O_2 + H_2O + 2e^- \Rightarrow 2OH^-$$

Assuming that diffusion of aqueous ions in thin films within the thin film plane is slower than gas diffusion out of the thin film (length:width >1), then these transport limitation could result in the localized build up of hydroxyl ions and increase in pH at the cathode and precipitation of minerals/salts. Within the last ten years several studies have investigated corrosion product precipitation on single metal substrates, for instance aluminum, magnesium and zinc. The minerals that form are functions of the gas phase composition, in particular CO_2, and the aqueous solution composition. As expected the corrosion products that form are a function of chloride and sulfate content of the aqueous solutions (Falk et al., 1998; Blucher et al., 2003; Linstrom et al., 2004). The net effects of these precipitation reactions at the cathodic sites are inhibition of oxygen reduction reaction by blocking of sites and the loss of water due to removal of aqueous ionic species due to mineral precipitation.

5.1 Brief literature review of thin film corrosion and resulting chemical transformations.

Thin film corrosion has been primarily studied at atmospheric conditions where thin film salt solutions arise from the drying of rain, condensation (dew), fog, snow, ocean spray,

and human activities (such as lawn watering). These atmospheric processes transport corrosive agents to the reactive metal surface. Corrosion under low temperature deliquescence conditions was first shown by Vernon (1932), who observed that gas phase ammonium sulfate particulates were able to induce corrosion of steel under moderate relative humidity conditions, while atmospheres devoid of particulate matter did not induce corrosion under the same conditions. Since the early 1920s, an entire field of atmospheric corrosion has developed. There are numerous texts that discuss atmospheric corrosion, such as Leygraf (2000).

5.2 Chemical Transformation Studies in Thin Brine Films in $CaCl_2$ and $MgCl_2$ Systems.
In this section we discuss chemical transformation studies conducted at LLNL. Prior to FY04, the majority of LLNL's thin-film electrolyte testing centered on calcium chloride system, because calcium chloride salts are predicted to deliquesce forming corrosive brines at temperatures in excess of 150˚C. However we observed that calcium chloride brines are unstable at elevated temperatures and low relative humidity due to HCl(g) volatility and the formation of non-deliquescent CaOHCl precipitate. Similarly corrosive magnesium chloride brines are not stable at elevated temperatures and low relative humidity. Our results suggest that these chemical transformations will lead to lower dry-out temperatures than predicted by the current Yucca Mountain Pitzer model (BSC 2004b). Below we review the calcium chloride and magnesium chloride chemical transformation experiments. More detailed results can be found in Hailey et al (2002) and the data are in DTN: LL030308812251.017, LL030309012251.018, and LL040702212251.113.

The chemical transformation of calcium chloride brines to dry precipitates is dependent on temperature on uncreviced Alloy 22 substrates. At 150˚C, calcium chloride brines destabilize within 24 hours due to HCl(g) volatility, solid phase precipitation, and water evaporation (Figure 10). All tests were conducted at 22 %RH. At 125˚C, the chemical transformation was evidenced by a gradual weight loss over one month. And at 100˚C $CaCl_2$ brine appeared to be stable over a period of 65 hours. The temperature dependence reflects lower HCl(g) volatility at lower temperatures. Electron microprobe analysis of the resulting precipitates (Figure 11) revealed they were composed of calcium, chloride, and oxygen. Thus, they are likely of the form $CaCl_x(OH)_{2-x}$. Lack of metal incorporation from Alloy 22 in the precipitates suggests that metal corrosion is not involved in the chemical transformation. This conclusion is supported by identical behavior of calcium chloride brines on inert glass substrates. Various substrates were therefore tested in conditions identical to the Alloy 22 experiment at 150˚C and 22%RH in order to probe the nature of the $CaCl_2$-substrate interaction (DTN LL020903812251.019).

Magnesium chloride brines are potentially more deleterious to the waste package material, as they form lower pH solutions than $CaCl_2$ brines. However, our results show that they are not stable above 115∞C and cannot sustain a deleterious aqueous solution within the drift environment. Testing initiated on Alloy 22 substrates at the same conditions as with $CaCl_2$ (150˚C, 22 %RH). In that environment, the $MgCl_2$ brine immediately evaporated, forming an insoluble scale. Testing at 125˚C resulted in total specimen dry-out in less than 24 hours. A final test at 115˚C was performed, which is below the thermal decomposition temperature of $MgCl_2$ of 118˚C (CRC, 1970).

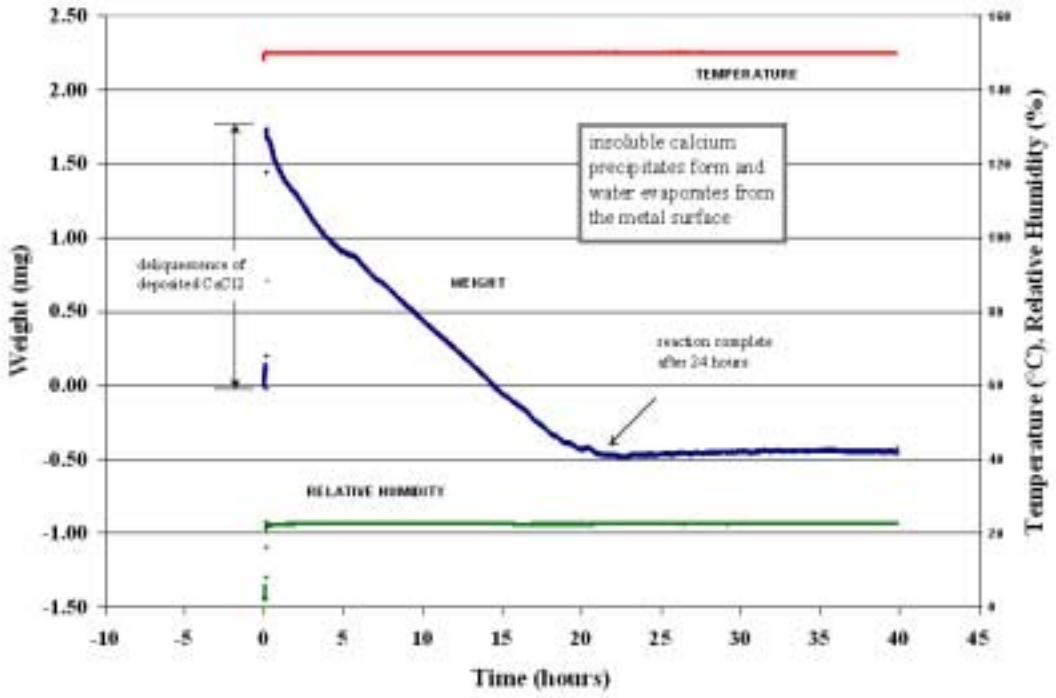

Figure 10. TGA data for $CaCl_2$ on Alloy 22 substrate, at 150˚C and 22%RH. [DTN LL030308812251.017]

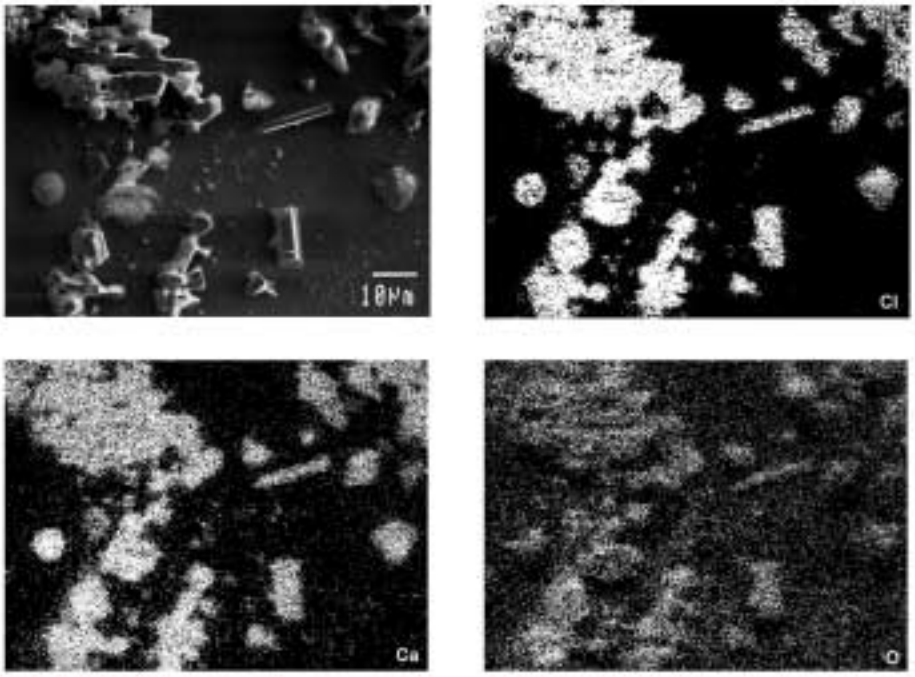

Figure 11. X-ray elemental mapping of precipitates formed from the reaction of $CaCl_2$ on the surface of Alloy 22 at 150˚C and 22%RH. SEM image is top left. [DTN LL030309012251.018]

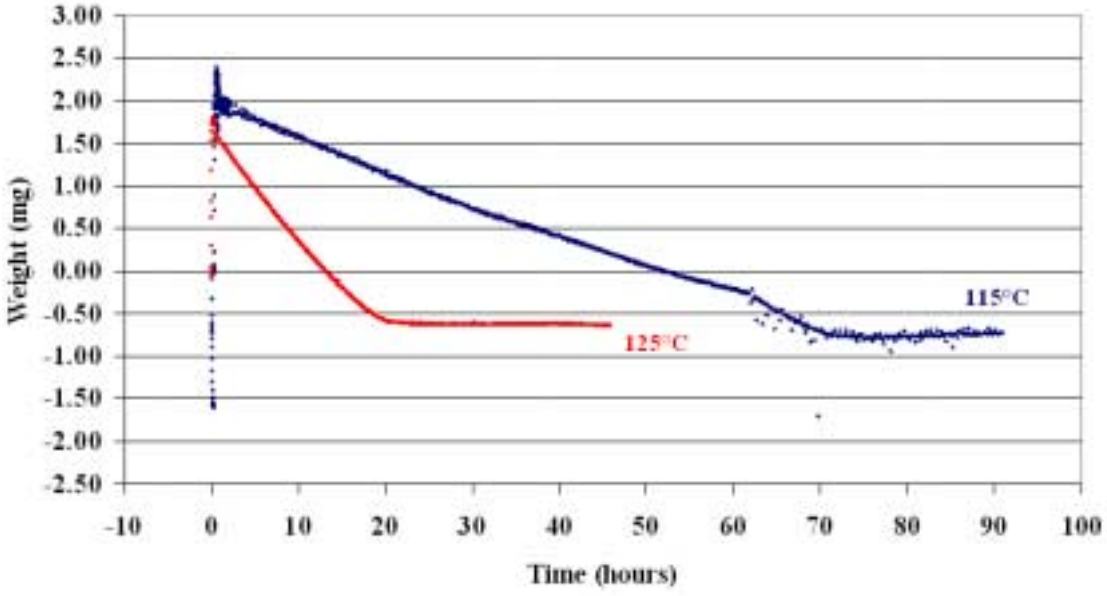

Figure 12**.** Gravimetric comparison $MgCl_2$ brines on Alloy 22 [DTN LL040702212251.113]

At 115˚C and 22 %RH, the $MgCl_2$ brine dried out within 72 hours (Figure 12). It is not clear whether the evaporation at this temperature was still due to thermal decomposition, or whether gas volatility was responsible for a chemical transformation within the brine. No corrosion of the Alloy 22 was observed.

5.3 Chemical Transformation Studies in Thin Brine Films of NaCl and NaCl-KNO3 brines

In FY04 testing shifted away from the more aggressive, less pertinent $CaCl_2$ and $MgCl_2$ brines, to chemistries that are more representative of those predicted within the proposed repository (see BSC 2004a and sections 2-4). Our working hypothesis for these NaCl and NaCl-KNO_3 brines, which have lower dry-out temperatures and lower chloride concentrations than the $CaCl_2$ and $MgCl_2$ brines, was that anodic corrosion would create an acid environment to promote gas volatility. The anodic reaction would be balanced by the cathodic diffusion of oxygen and the creation of more alkaline solutions. These alkaline solutions would then promote diffusion of CO_2(g) and the precipitation of Na_2CO_3 and K_2CO_3 solids, drying out the brine and shutting down corrosion. We employed three types of experiments to test this hypothesis. One type of experiment tested chemical transformations in the absence of crevice formers to establish a background for the brine stability. The second type of experiment used crevice formers to drive the initial corrosion and create an acid environment. We also conducted crevice corrosion experiments using $CaCl_2$ brines to compare with the chemical transformations observed in $CaCl_2$ brines in the absence of crevice formers. The third type of experiment measured the rate of CO_2(g) diffusion in alkaline NaCl brines. In contrast to the $CaCl_2$ and $MgCl_2$ brines where chemical transformations resulted in dry-out, which shuts off corrosion in high temperature and low relative humidity environments, the more common NaCl and NaCl-KNO_3 brines were stable. However, there is some preliminary evidence that suggests that the corrosion potential is lower in thin layers of brine than in bulk solutions.

5.3.1 Methods

The thin film chemical transformation experiments were conducted in a thermogravimetric analyzer (Cahn TG-100) modified to achieve 23 %RH at 150˚C. Humidity was achieved and controlled by varying the ratios of dry air and saturated air. Sensors within the sample chamber measured temperature and relative humidity continuously. Specimen mass (± 1mg) was recorded as a function of time to track chemical transformations among the brine film and Alloy 22. Specimens (50mm x 13mm x 1.5mm) were generally polished to a mirror finish, with a final polish of 1mm Al_2O_3. Dilute salt and mixed-salt solutions were sprayed into a coating chamber as an aerosol for uniform specimen coating. Immediately following the coating process, specimens were placed in the sample chamber and dried at the run temperature and a very low relative humidity (nominally < 2%RH). The balance was then tarred and the relative humidity in the sample chamber was increased to the run set point, which was always above the deliquescence relative humidity for the given brine composition. Throughout each test, specimen weight change was recorded as a function of time, and physical changes on the surface were monitored visually. Test duration ranged from 24 hours to 30 days, depending on the reaction rate. Both Alloy 22 and Incoloy 825 were used as

metal substrates in the tests. Optical interferometry, optical microscopy, and SEM imaging were used to analyze changes in substrate surface morphology.

A part of our program included electrochemical tests to induce corrosion and promote chemical transformations by creating an acid environment to promote HCl(g) volatility. These were not easy experiments to do and most of our time was spent on testing various design concepts. High temperature electrochemical testing in thin-film brines requires a system capable of maintaining stable environmental conditions, as well as methods for achieving and sustaining the brine film, and ionically bridging the test electrolyte to the reference electrode at room temperature. An environmental chamber was used to control and monitor temperature and relative humidity. Crevice formers were also used to simulate localized corrosion. Prior to testing, the specimen was polished to a mirror finish, with a final polish of 1mm Al_2O_3. The sample was placed into its holder, and electrolyte solution was introduced on the top surface of the horizontally mounted specimen, in a layer of sufficient thickness (~3-5mm) to overcome surface tension and allow wetting of the entire metal surface. A thermocouple attached to the bottom surface of the specimen measured the specimen temperature. Sensors were placed within the specimen holder region to environmental conditions to measure experimental temperature and relative humidity. The open circuit potential was monitored with reference electrode (Ag/AgCl). Due to the high temperature of the test environment, the reference electrode was kept outside of the environmental chamber. A customized Luggin probe filled with saturated electrolyte solution provided a salt bridge between the test solution and the reference electrode.

5.3.2 Results and Discussion

5.3.2.1 TGA Experiments

We attribute the lack of chemical transformation of thin NaCl and mixed NaCl-KNO_3 brine films to lower HCl(g) volatility at 105˚C and 120˚C in brines with near neutral pH and lower chloride concentrations (and high NO_3:Cl for the NaCl-KNO_3 salt mixture) than the $CaCl_2$ or $MgCl_2$ brines discussed above. In non-creviced samples, no chemical transformations were observed and no evidence of corrosion was observed on the polished Alloy 22 or Incoloy 825 samples. Sodium chloride brines were tested at 105˚C and 78 %RH, a few degrees below the boiling point and slightly above the deliquescence relative humidity of the pure salt. The NaCl brine remained stable in this environment during a one-month test on Alloy 22 substrate and for two weeks on Incoloy 825. No visible change to the surface of the specimen was detected. We conducted one test on Incoloy 825 specimen at 120˚C and 42%RH in NaCl-KNO_3 solution with a NO_3:Cl of about 35 m : 6 m. These conditions correspond to the eutectic composition for NaCl-KNO_3 salt mixture. Over a two-week period, a very slight (almost negligible) weight loss was observed. As in the case of the pure NaCl electrolyte test, no corrosion was observed on the polished regions of the specimen, although slight general corrosion was apparent in regions of high surface roughness.

A major focus in FY04 was to incorporate crevice formers into the TGA tests to initiate corrosion and create an acid environments that might promote gas volatility and chemical transformations. Three tests were performed with ceramic crevice formers. Incoloy 825 tests with NaCl at 105˚C and 78%RH, using bare ceramic crevice formers showed evidence of corrosion, but no evidence of chemical transformations. Over a

period of two weeks, a very slight (negligible) weight loss was observed. Post-test analysis revealed several isolated cases of crevice corrosion beneath some of the ceramic teeth. Optical microscopy also indicated the presence of some kind of organic film around the teeth, most likely due to contamination from the non-sterile crevice former.

Incoloy 825 was reacted with $CaCl_2$ at 150˚C and 22%RH using a ceramic crevice former that had been coated with Teflon tape. In these samples, the brine film was present on the bulk sample as well as under the crevice former. Although dry-out occurred fairly swiftly, and a gradual weight loss was observed over a period of 48 hours, there also appeared to be unreacted brine in the creviced regions. Post-test analysis revealed evidence of crevice corrosion beneath all crevice teeth (Figure 13).

Alloy 22 was tested with $CaCl_2$ at 150˚C and 22%RH, using a ceramic crevice former coated with a thicker Teflon sheet, as the Teflon tape used in the Incoloy 825 test had proven too thin to withstand compression, and had been penetrated in several areas. Again, a gradual dry-out was observed over a 48-hour period. Post-test analysis revealed no evidence of corrosion anywhere on the Alloy 22 specimen (Figure 13). As with the Incoloy 825 test, there appeared to be unreacted $CaCl_2$ remaining in the creviced regions. One possible interpretation of these preliminary results is that gas volatility is inhibited by the narrow crevice gap width, and that the overall weight loss and represent dry-out on the bulk sample (i.e. non-creviced sample).

5.3.2.2 *Open Circuit Experiments*

Open-circuit tests performed a creviced Alloy 22 specimens, using a thin layer of 6.8 m NaCl at 105˚C and 78 %RH yielded a more passive stable film than in bulk solutions at 90˚C. In the first test, the open circuit potential went from –300 mV at the start of the experiment to 0 mV after 250 to 350 ours of reaction (Figure 14). Post-test analysis of this sample revealed evidence of crevice corrosion beneath ~ 5% of the creviced area (Figure 15). The second test was allowed to run for only 32 hours. During this short time period, the open circuit potential went from –275 mV to 90mV and the end of the experiment. No significant crevice corrosion was observed on this sample. By way of comparison, long-term Alloy 22-rod samples were tested in bulk 4M NaCl at 90°C (DTN: LL040402212251.084). Open circuit values for specimens in aerated conditions were consistently lower than those observed for the thin film case, at -100mV versus Ag/AgCl. This may be explained by 1) shorter oxygen diffusion path length through the thin film than through a bulk solution, and/or 2) faster/denser formation of Cr_2O_3 at the higher temperatures in the thin film tests than in the bulk solution tests.

5.3.2.3 CO_2(g) diffusion in alkaline NaCl brines

We observed no diffusion of CO_2(g) in alkaline NaCl brines over a one-month period (data are recorded in DTN: LL040604923121.040). Diffusion was calculated by measuring the total dissolved carbonate, which has a very high solubility in alkaline solutions, as a function of time. In all cases the amount of total dissolved carbonate was equal to the amount present in the NaOH base added to the NaCl brine to create the alkaline environment. These results suggest that any chemical transformations of NaCl-KNO_3 brines to insoluble carbonate minerals will be controlled by reaction kinetics.

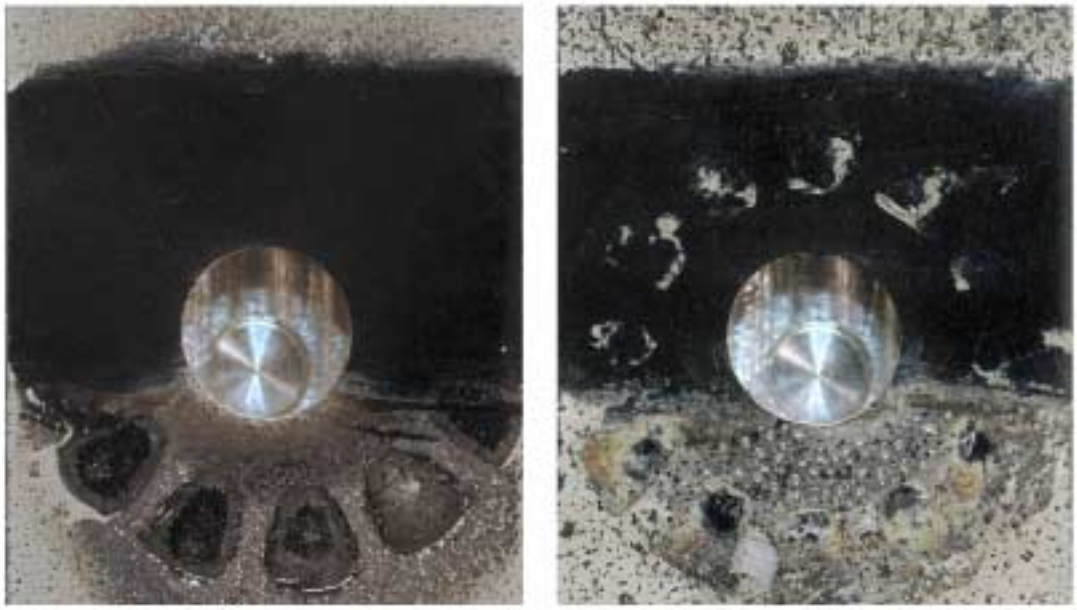

Figure 13. Post-test images of Alloy 22 (left) and Incoloy 825 (right) specimens after reaction with CaCl2 at 150C and 22%RH. Footprints of the ceramic crevice former teeth are visible at the bottom of both samples due to salt dispersion variance; however, when cleaned, only Incoloy 825 shows signs of crevice corrosion. [DTN LL040702212251.113]

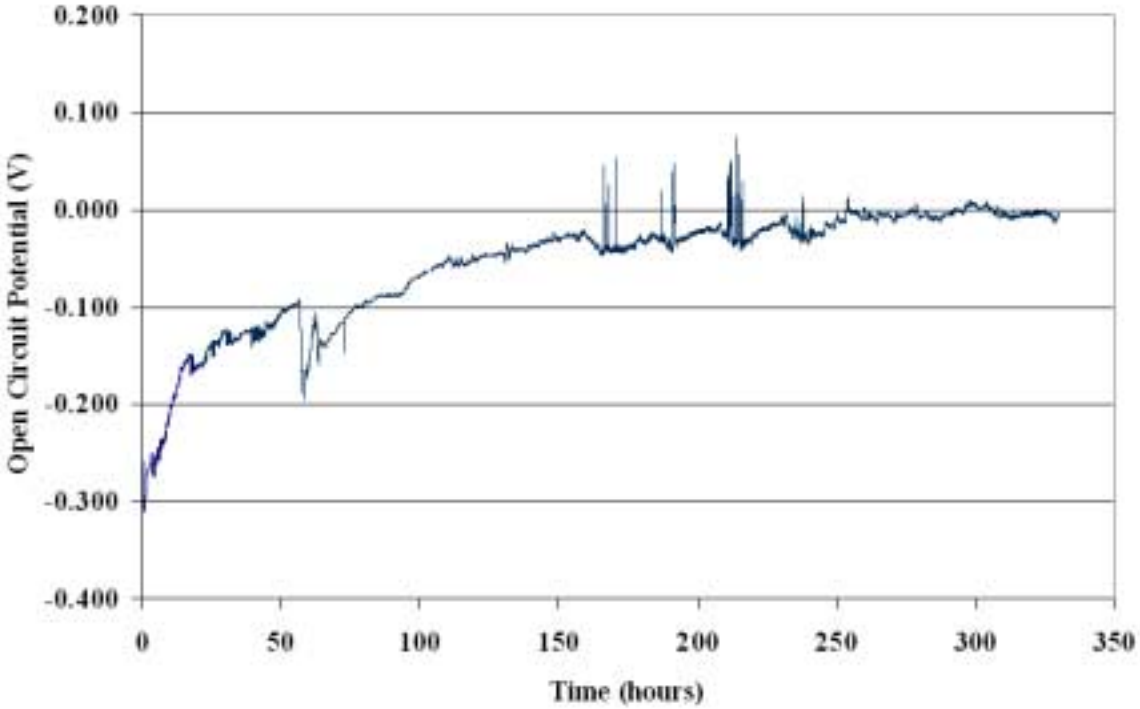

Figure 14. Open circuit potential curve for Alloy 22 in thin aqueous layer NaCl electrolyte at 105˚C and 78%RH. [DTN LL040702112251.112]

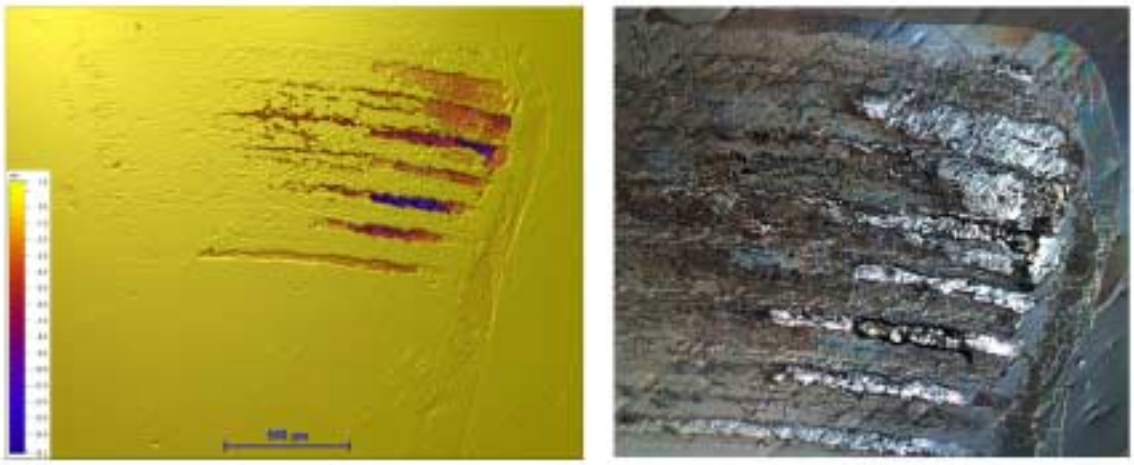

Figure 15. Interferometry images (left) and optical micrographs of crevice corrosion on Alloy 22. NaCl electrolyte (~6.75*m*), 105˚C and 78%RH for two weeks at open circuit. [DTN LL040702112251.112]

5.4 Implications for localized corrosion at elevated temperatures

Our results suggest that chemical transformations do not play a significant role in the stifling of corrosion of Alloy 22 in NaCl and NaCl-KNO_3 brines and that YMP corrosion models based on bulk experiments can be used to predict waste package corrosion provided that solution chemistry is adequately represented in the corrosion model. At this time, it is not clear if chemical transformations will play a key role in predicted NaCl-KNO_3-$NaNO_3$ and NaCl-KNO_3-$NaNO_3$-$Ca(NO_3)_2$ brines (BSC 2004a), because in the absence of corrosion, these brines are stable at much higher temperatures than previously modeled.

6.0 Composition of evaporating seepage waters at waste package surfaces

Temperatures at the drift wall are predicted to be below the boiling point of dilute pore waters after about 1000 years. The assessment of water chemistry that may contact the waste package surfaces requires the calculation of a wide range of water composition over very long time periods (1000 to 100,000 years) in environments where temperature and relative humidity will change as the repository heats up and cools back down to ambient conditions. Understanding and verifying the chemical divides that control brine composition as seepage water evaporates are important to placing boundaries on the corrosiveness of the chemical environment to waste package materials. We have conducted a series of experiments that explore the geochemcial controls for the concentration of these dilute waters to brines as they evaporate at the hotter waste package surface.

We have adopted the chemical divide theory used to described saline lake geochemistry (Eugster and Hardie 1978, Drever 1997, and Eary 1998) to evaluate the evolution of Yucca Mountain seepage waters at the waste package surface. The chemical divide theory generally describes the chemical evolution of dilute waters upon evaporation in terms of their equivalent calcium, sulfate and bicarbonate ratios and is shown in Figure 16. The chemical evolution of evaporating water is controlled by the

high solubility of salt minerals relative to the moderate solubility of calcium sulfate and low solubility of calcium carbonate minerals. An alkaline pH, bicarbonate brine (Na-K-**CO_3**-Cl-SO_4-NO_3) forms from dilute waters with dissolved calcium concentrations that are less than dissolved carbonate (Ca < HCO_3+CO_3, equivalent %). A near neutral pH, sulfate brine (Na-K-Mg-Cl-**SO_4**-NO_3) forms from dilute waters with dissolved calcium concentrations that are greater than the dissolved carbonate, but less than the combined dissolved sulfate and carbonate concentrations (Ca < SO_4+HCO_3, equivalent %). A calcium chloride brine with more acid pH (Na-K-**Ca**-Mg-Cl-NO_3) forms from dilute waters with a dissolved calcium concentration that is greater than the combined dissolved sulfate and carbonate concentrations (Ca > SO_4+HCO_3, equivalent %). The measured compositions of Yucca Mountain pore water vary, but can be generally classified as waters that should evolve towards sulfate and sodium bicarbonate brines, with a few calcium chloride brines as they evaporate (Figure 16).

In this report we focus on the brine chemistry formed by the evaporation of a synthetic Yucca Mountain sulfate, bicarbonate and calcium-chloride pore waters between 87ºC and 95ºC over a concentration range of 1x to ~3500x or a relative humidity range of 100% to 72%. Specifically we will discuss important chemical divides that effect corrosion of the waste package surfaces, evidence for gas volatility from the evaporating pore water, and the ability of EQ3/6 geochemical code and the Yucca Mountain Program Pitzer model to predict the in-drift aqueous chemical environment. Details of the experimental method and the results for evaporation of the sulfate and bicarbonate pore water can be found in Alai et al. (2005) and in Sutton et al. (2004). Data supporting this report is available in the following DTNs for the evaporation of sulfate, bicarbonate and calcium chloride waters: LL030107023121.019, LL030107123121.020, LL030106923121.018, LL030408523121.028, LL031005723125.007, LL040307623121.038, LL040905823121.043, LL040905923121.044.

6.1 Methods

Synthetic pore waters were evaporated up to 3400 times at 87ºC or 95ºC in a series of experiments to iteratively concentrate the solution (legs 1, 2, 3, etc). For the sulfate and calcium-chloride waters a fixed volume of water was evaporated in each leg, and for the bicarbonate water the evaporating water was replaced with the dilute starting water in an effort to extend the concentration range of each leg. The solutions were prepared at room temperature using analytical grade salts.

Evaporation was conducted in a vented halar lined vessel heated to temperature in a fluidized sand bath furnace. Extent of evaporation was monitored by collecting the condensed water vapor or by the ratio of measured to initial NO_3 concentrations. Periodic samples of the evaporating solution were filtered at 95^{o}C and analyzed to determine the water chemistry. After the last sample was taken for each leg, the evaporation was continued to dryness. The solid precipitate was collected at the end of each leg of the experiment for powder X-ray diffraction (XRD) analysis.

Solution compositions were modeled using EQ3/6 geochemical code (Wolery and Jarek, 2003) and a high temperature Pitzer ion-interaction model (BSC, 2004b). The predictive models were generated to mirror the experimental design and analysis. The evaporation model consisted of three steps. In the first step, the measured composition of

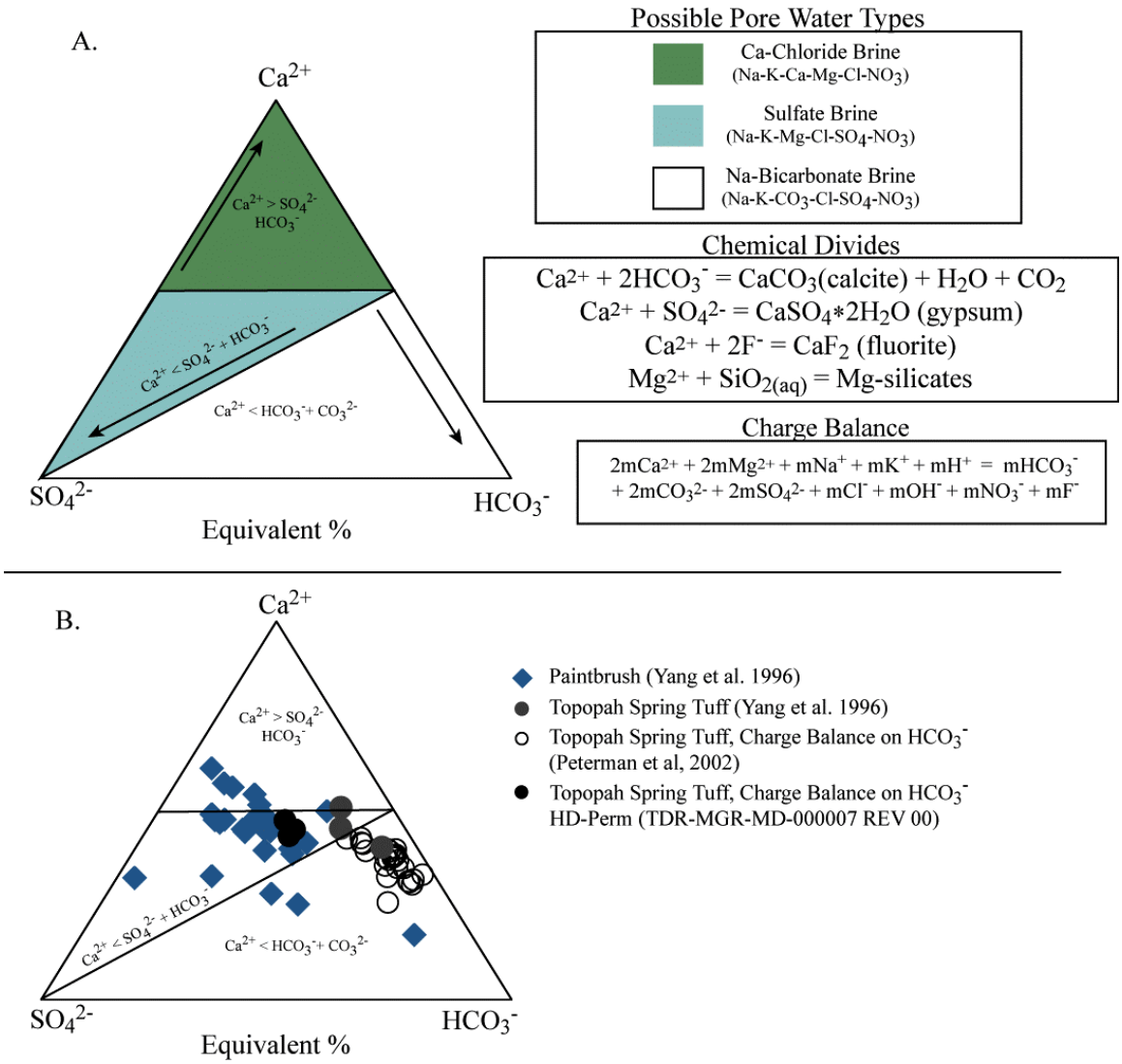

Figure 16. A. Calcium carbonate and calcium sulfate chemical divides for evaporation of dilute waters. B. Yucca Mountain, NV pore waters as measured.

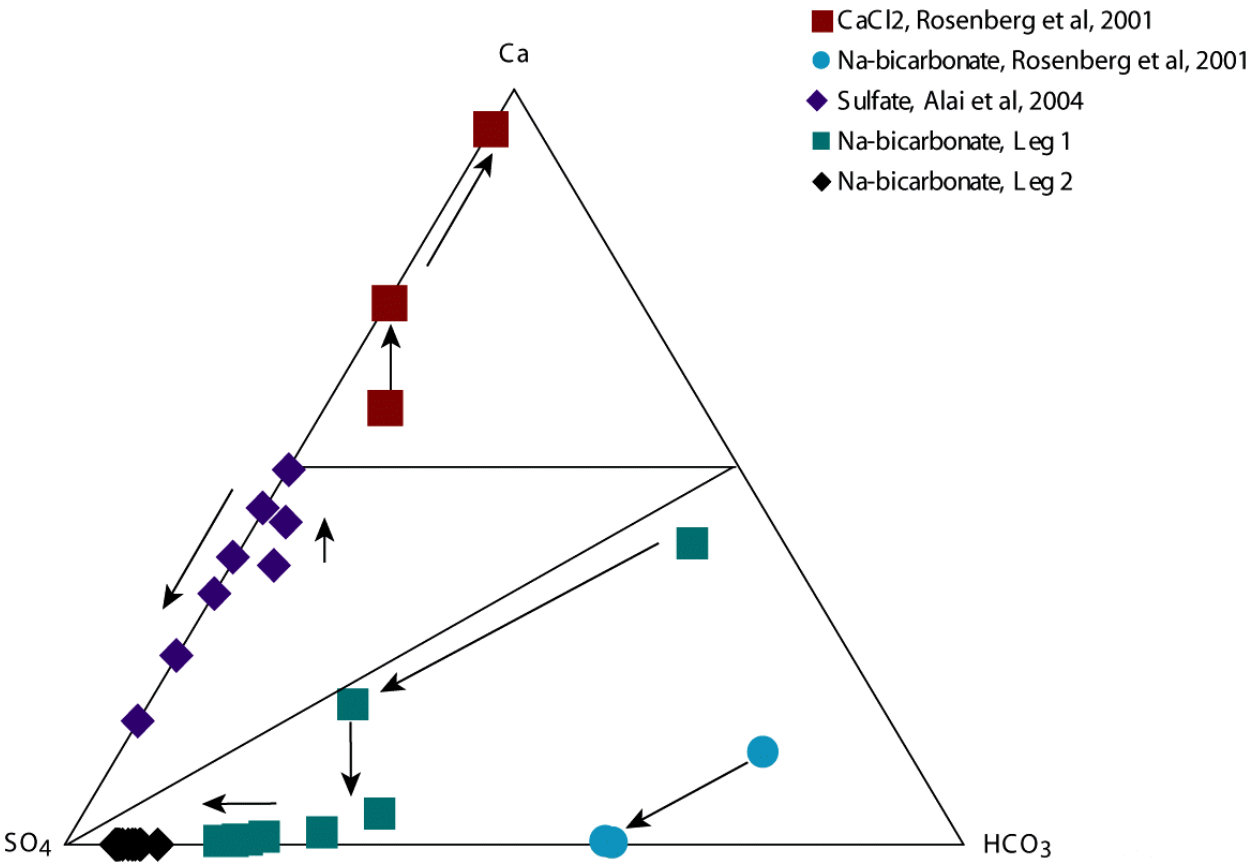

Figure 17. Chemical composition of dilute calcium chloride (synthetic Topopah Spring tuff pore water, Rosenberg et al, 2001), Na-bicarbonate (synthetic J-13 groundwater, Rosenberg et al, 2001), sulfate (synthetic Topopah Spring tuff pore water, Alai et al, 2004), and Na-bicarbonate (Synthetic Topopah Spring tuff pore water, this study) waters upon evaporation.

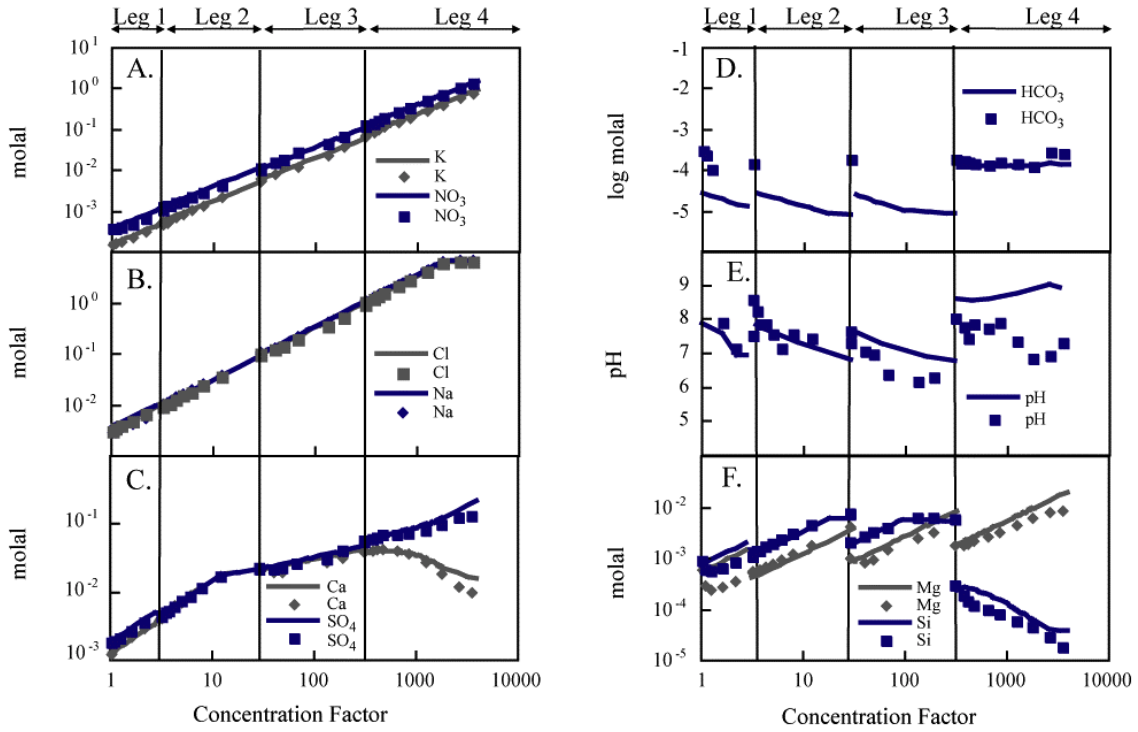

Figure 18. Evaporation of dilute sulfate water based on a Topopah Spring tuff pore water chemistry. Comparison of experimental and model solution concentrations vs. concentration factor. Symbols indicate experimental data and lines indicate model data.

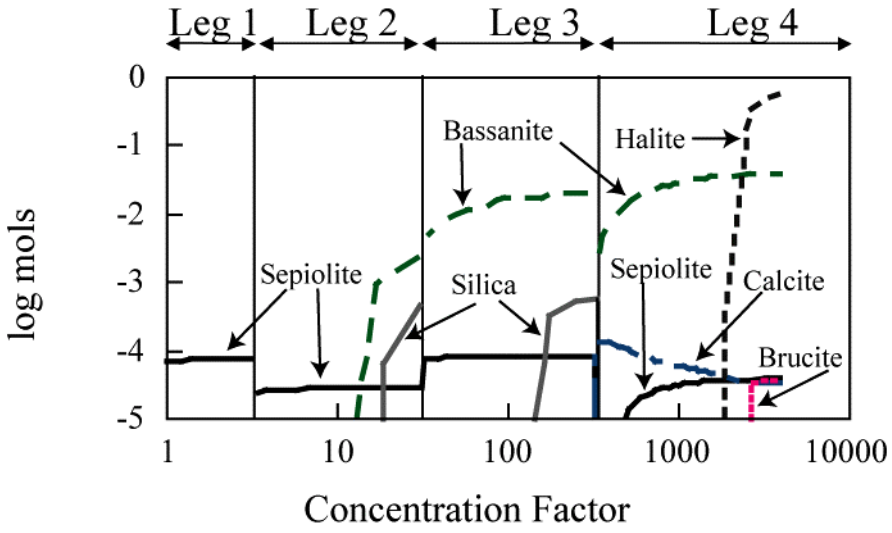

Figure 19. Evaporation of dilute sulfate water based on a Topopah Spring tuff pore water chemistry. Predicted mineral amounts vs. concentration factor.

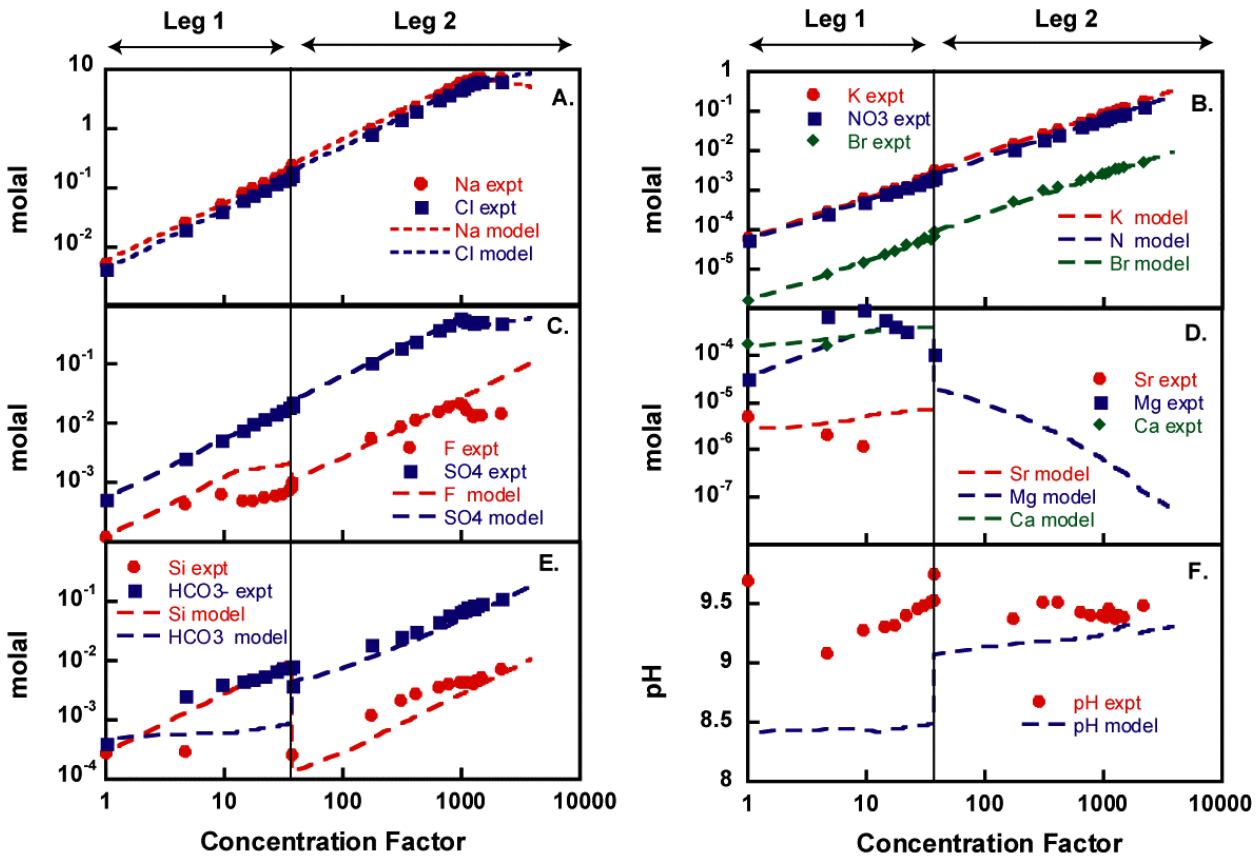

Figure 20. Evaporation of dilute Na-bicarbonate water based on a Topopah Spring tuff pore water chemistry. Comparison of experimental and model solution concentrations vs. concentration factor. Symbols indicate experimental data and lines indicate model data.

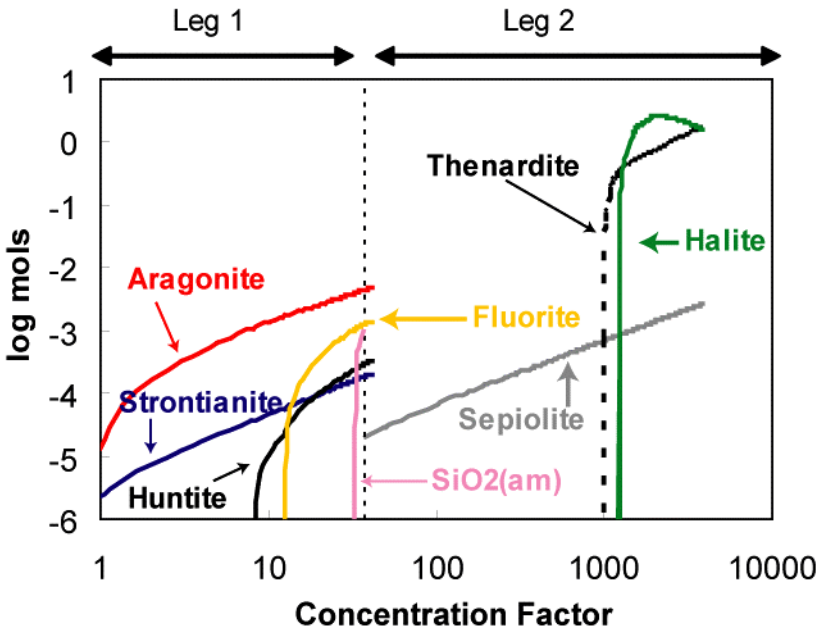

Figure 21. Evaporation of dilute Na-bicarbonate water based on a Topopah Spring tuff pore water chemistry. Predicted mineral amounts vs. concentration factor.

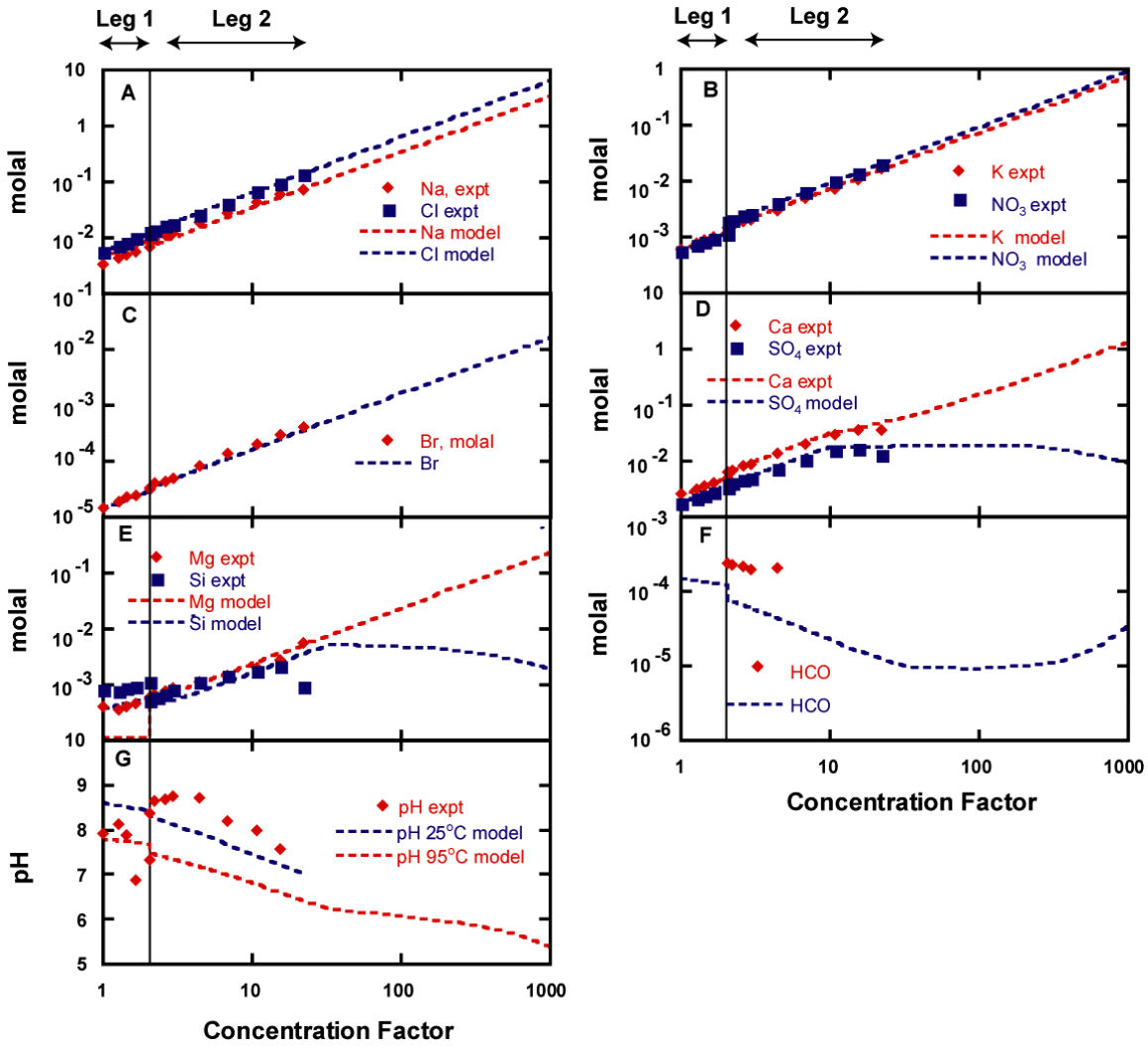

Figure 22. Evaporation of dilute calcium chloride water based on a Topopah Spring tuff pore water chemistry. Comparison of experimental and model solution concentrations vs. concentration factor. Symbols indicate experimental data and lines indicate model data.

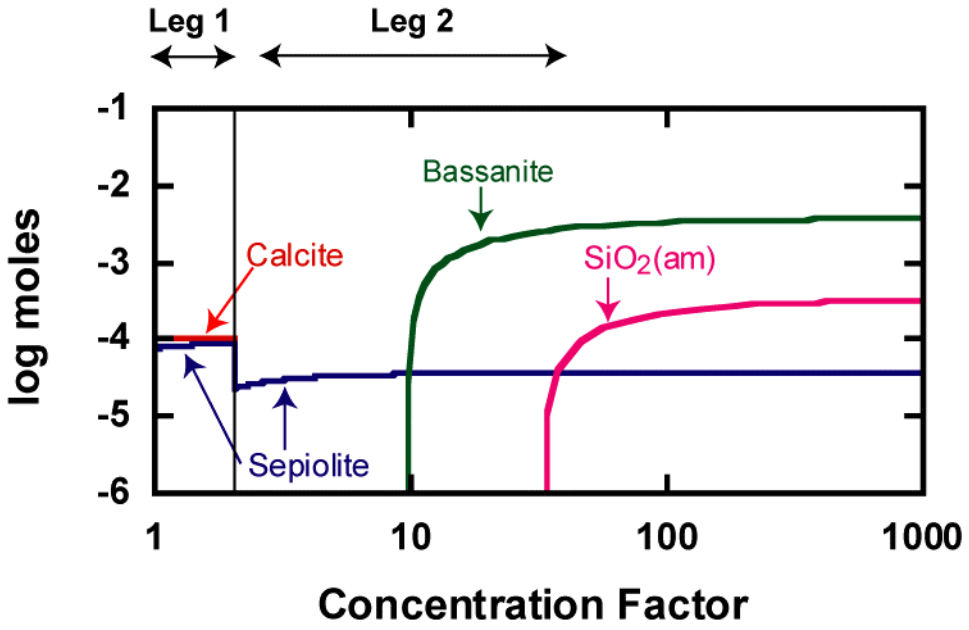

Figure 23. Evaporation of dilute calcium chloride water based on a Topopah Spring tuff pore water chemistry. Predicted mineral amounts vs. concentration factor.

the first sample at temperature was speciated, suppressing all mineral precipitation in the calculation. During the second step, the speciated water was evaporated at temperature by stepwise removal of solvent water. In the evaporation step, all minerals were allowed to precipitate with the exception of quartz and dolomite because of slow kinetics; glaserite, hydromagnesite and magnesite because the available thermodynamic data are questionable; and cristobalite because it forms above 1470ºC. In the speciation and evaporation steps, oxygen and carbon dioxide fugacity were fixed at 21% and 0.033% respectively to simulate atmospheric experimental conditions. A CO_2(g)-sink was added to the model to remove excess buildup of CO_2(g) from the reaction surface. Finally, in the third step, the predicted pH values at temperature were corrected to 25°C to compare to measured pH at room temperature in an additional simulation in which all mineral precipitation was suppressed and $\sum CO_2$(aq) was fixed to the predicted value at temperature.

6.2 Important chemical divides

Figure 17 shows that dilute sulfate, bicarbonate, and calcium-chloride pore waters yield their respective sulfate, bicarbonate, and calcium-chloride brines as predicted by chemical divide theory based on their initial $Ca:SO_4:HCO_3$ ratio (Figure 17). Although these waters are classified as a sulfate, bicarbonate, and calcium-chloride brines, the water chemistry is dominated by sodium and chloride. In the final sulfate brine, sodium and chloride are 45 and 40 equivalent % respectively while calcium and sulfate are relatively minor constituents at 0.2 and 1.6 equivalent % respectively. In the final bicarbonate brine, sodium and chloride are 49 and 44 equivalent % respectively while carbonate is a relatively minor constituent at 0.8 equivalent %. However, in the calcium-

chloride brine (at 22x or 99.5 %RH) chloride is balanced by calcium (50 equivalent %) and by sodium (50 equivalent %). Extension of the modeling to 1000x yields a mixed brine with significant amounts of dissolved calcium, magnesium, sodium, potassium, and chloride and nitrate (see last paragraph in section 6.2; section 6.4).

Chemical divides are shown for the evaporation of the sulfate water in Figures 18 and 19, the bicarbonate water in Figures 20 and 21, and the calcium-chloride water in Figure 22 and 23 as a comparison of the modeled and experimental water chemistry and the predicted mineral precipitation as a function of the concentration factor. For the sulfate water, halite, bassanite (or other calcium sulfates), magnesium silicate, amorphous silica, and possibly fluorite and brucite solubility control brine chemistry based on model predictions and experimental results (Figures 18 and 19). The most corrosive component of the sulfate brine is the high concentrations of chloride, which are controlled by the solubility of halite. The concentration of calcium and magnesium are limited by the solubility of sulfate and magnesium silicate minerals, preventing the formation of a potentially corrosive calcium and magnesium chloride brines. Similarly, the removal of fluoride (presumably as fluorite) from the starting solution prevents the formation of a potentially corrosive fluoride containing brine. High nitrate to chloride ratios in this sulfate brine may further limit corrosion of the waste package materials (BSC 2004c).

For the bicarbonate water, aragonite, thenardite, halite and possibly strontianite, huntite, sepiolite, amorphous silica and fluorite solubility control brine chemistry based on experimental results and model predictions (Figures 20 and 21). Similar to the sulfate brine, the most corrosive component of the bicarbonate brine is the high concentration of chloride, which is controlled by the solubility of halite. The concentration of calcium and magnesium are limited by the solubility of carbonate and magnesium silicate minerals, preventing the formation of a potentially corrosive calcium and magnesium chloride brines. In contrast to the sulfate brine, fluoride concentrates in these solutions until its solubility is controlled by fluorite at 12x and by an unidentified phase a 1000x. Our results indicate that model predictions of fluoride concentrations will exceed those in the in-drift environments for bicarbonate brines. Although bromide is corrosive constituent that is not limited by mineral solubility, it is present in minor amounts even in more concentrated brines. At the end of this experiment (2140x), the bromide concentration (0.005 m) is more than 1000 times smaller than the chloride concentration (6.4 m). Nitrate to chloride ratios tend to be below the nominal ratio of NO_3:Cl = 0.5 that is known to limit corrosion of the waste package materials (BSC 2004c).

Similar to the sulfate water, halite, bassanite (or other calcium sulfates), calcite, sepiolite and amorphous silica solubility control calcium-chloride brine chemistry based on experimental results and model predictions (Figure 22 and 23). However, calcium is predicted to continue to concentrate in solution and becomes a significant dissolved component as the dilute evaporates because the initial $Ca:SO_4 > 1$. Magnesium concentrations are also predicted to concentrate as the solution pH decreases with evaporation because sepiolite solubility increases at more acid pH. Consequently, calcium-chloride brines have a higher potential to corrode the waste package surface compared to the sulfate and bicarbonate brines. The corrosiveness of the solution may be mitigated by dissolved nitrate. At 1000x, predicted NO_3:Cl = 0.14. This value will increase as the brine continues to evaporate, because chloride concentrations will be limited by halite solubility and nitrate concentrations will increase until niter solubility is

reached. Our interpretation of the "corrosiveness" of calcium-chloride brines is based primarily on model predictions that extend will beyond the experimental data. Additional concentration experiments are need from 20 to 3000x to validate the model calculations.

6.3 Gas volatility in evaporating pore water

Evaporation of concentrated calcium chloride solutions around 140°C observed significant volatilization of HCl(g) as measured by acidic condensates (Pulvirenti et al. 2003). The results from our previous experiments indicated that gas volatility is not a major concern for the evaporation and concentration of sulfate and bicarbonate waters (Alai et al, 2005; Sutton et al., 2004). In those two sets of experiments, measured water vapor condensates were below the detection limit for all analyzed ions. The condensates for evaporation of this calcium-chloride water were below the detection limit for all analyzed ions with the exception of the last condensate sample at a concentration factor of 22X. Measured chloride concentration for this last sample was 1ppm. Also, the pH of the condensate dropped from neutral to pH =4.7. No other anions or cations were detected in the condensate. This indicates that HCl(g) was trapped in the condensate at these conditions as calcium-chloride water evaporates. Although this interpretation is based on the analysis of the final solution, it is likely that gas volatility will continue as calcium-chloride solutions concentrate. Evidence of gas volatility in this evaporation experiment and the destabilization of pure $CaCl_2$ brines at 150˚C and 22 %RH (see section 5) suggests that chemical transformations may also destabilize a mixed Ca-Mg-K-Na-NO_3-Cl brine (although this has not been tested).

6.4 Comparison of model predictions and experimental data

Evaporation of sulfate, bicarbonate, and calcium-chloride waters provide benchmark data needed to both understand the brines and salts that form upon evaporation of varied waters and to validate the EQ3/6 geochemical code and a high temperature Pitzer model used to predict the in-drift environment aqueous chemistry at waste package surfaces over the thermal history of the repository (BSC 2004b). Our results show that predicted brine chemistry agree with experiment within a factor of two from most elements. Discrepancies with pH, total dissolved carbonate, magnesium, and silica are somewhat larger. Predicted mineral precipitates also agree with experiment for all cases where enough mineral formed to be detected by x-ray diffraction. Below we summarize the match between model prediction and experiment for the dissolved constituents as the dilute waters evaporate to brines. These comparisons are shown in Figures 18-22.

We observe excellent agreement between model and experiment for dissolved constituents that concentrate conservatively and those that are controlled by halite or sulfate solubility. Figures 18, 20, and 22 show that dissolved potassium, nitrate and bromide concentrate linearly in each experiment, because the brines are under saturated with respect to the highly soluble nitrate and bromide salts. Dissolved chloride concentrations increase until the brines are saturated with respect to halite, and dissolved sodium concentrations increase until they are saturated with respect to halite and/or thenardite. Similarly, the agreement between model and experiment for calcium and sulfate concentrations is quite good when their concentrations are controlled by the solubility of bassanite (or other calcium sulfate minerals). The good agreement between

model and experiment for sodium, potassium, chloride, and nitrate at first glance appears to be at odds with the large discrepancies reported for the deliquescence of NaCl-KNO_3 salts (Carroll et al., 2005; section 2). The high Na:K and Cl: NO_3 mole ratios seen in the evaporation experiments appear to effectively mask any mismatch due to use of constant temperature parameters for K^+-NO_3^- interactions in the Pitzer model. When brines are saturated with niter (KNO_3), then K^+-NO_3^- interactions will be very more important and we expect a significant mismatch between model and experiment. In the early legs of two of the experiments, the model under predicts sodium concentrations. This observation is explained by the over-prediction of positively charged magnesium, and the subsequent decrease in sodium to neutralize the charge.

Generally, the ability of the model to match the experimental data is poorer for the minor constituents. The factor of two discrepancy between model and experiment for magnesium and silica solubility translates to absolute concentrations of less than 0.01 molal for most of the brines. This agreement suggests that the use of sepiolite to model magnesium and silica concentrations, and the Pitzer model are adequate for the evaporation of waters in a repository environment to about 70% relative humidity. Uncertainty in the sepiolite solubility product is well defined at temperatures less than 100ºC, with log K_{sp} = 24 (±0.3) at 95ºC ($Mg_4Si_6O_{15}(OH)_2 \cdot 4H_2O + 8H^+ = 4Mg^{2+} + 6SiO_2(aq) + 11H_2O$) (Helgeson et al., 1978). This translates to less than 10% uncertainty. Better models may be required to match dissolved magnesium concentrations in more concentrated brines. The current model suggests that magnesium will concentrate as the brines become more acid, due to the strong dependence of sepiolite solubility on pH. Given the potential corrosiveness of calcium and magnesium chloride brines, the model needs to be validated with experimental data beyond 22x of the current calcium-chloride study.

The Yucca Mountain database appears to lack important thermodynamic data for fluoride minerals. In the bicarbonate brines, modeling results over predict fluoride concentrations at 12x and again at 1000x. Unfortunately the amount of the fluoride-containing phase was too small to be identified by XRD. One possibility is the precipitation of kogarkoite ($Na_3(SO_4)F$) that has been identified in drip experiments using a 100x synthetic sodium bicarbonate water (Nguyen et al., 2003). We assume that the extremely low solubility of fluorite controls fluoride concentrations, because it precipitated from the starting sulfate water as the water was heated to levels below the analytical detection limit. Similarly, no fluoride was detected in the measured pore water that was the basis for the starting calcium-chloride water (Yang et al., 1996)

Total dissolved carbonate concentrations and pH are strongly tied to each other. In all of our experiments concentration of total dissolved carbonate was constrained by assuming atmospheric pCO_2, because filtered air was continually flowed over the water surface to promote evaporation. In the last legs of the sulfate and bicarbonate waters, the good match between model and experiment total dissolved carbonate supports this constraint. However, earlier legs of these experiments and in the calcium-chloride waters, there can be as much of as an order of magnitude difference between model and experiment. Model prediction of pH is typically within one order of magnitude of the experimental results. In higher ionic strength solutions, the measured pH is conditional because the high salt concentrations interfere with the electrode measurement. The factor of 10 discrepancy in pH does not appear to have a significant impact on the corrosiveness

of the sulfate and bicarbonate brines because sulfate precipitation is independent of pH and aragonite becomes less soluble with increasing pH during the evaporation process. More importantly, the initial calcium concentration is less than the combined sulfate and bicarbonate concentrations, which results in the removal of dissolved calcium as these waters concentrate. The inability of the model to capture experiment pH in the calcium-chloride waters may be more problematic, because these waters become more acid with evaporation increasing the solubility of magnesium silicates, as we have already discussed.

7.0 Summary

We have conducted a series of deliquescence, boiling point, chemical transformation, and evaporation experiments to determine the composition of waters likely to contact waste package surfaces over the thermal history of the repository as it heats up and cools back down to ambient conditions. In the above-boiling period, brines will be characterized by high nitrate to chloride ratios that are stable to higher temperatures than previously predicted. This is clearly shown for the NaCl-KNO_3 salt system in the deliquescence and boiling point experiments in this report. Our results show that additional thermodynamic data are needed in nitrate systems to accurately predict brine stability and composition due to salt deliquescence in dust deposited on waste package surfaces. Current YMP models capture dry-out conditions but not composition for NaCl-KNO_3 brines, and they fail to predict dry-out conditions for NaCl-KNO_3-$NaNO_3$ brines. Boiling point and deliquescence experiments are needed in NaCl-KNO_3-$NaNO_3$ and NaCl-KNO_3-$NaNO_3$-$Ca(NO_3)_2$ systems to directly determine dry-out conditions and composition, because these salt mixtures are also predicted to control brine composition in the above-boiling period. Corrosion experiments are needed in high temperature and high NO_3:Cl brines to determine if nitrate inhibits corrosion in these concentrated brines at temperatures above 160°C.

Chemical transformations appear to be important only for pure calcium- and magnesium-chloride brines at temperatures greater than 120°C. This stems from a lack of acid gas volatility in NaCl/KNO_3 based brines and by slow CO_2 (g) diffusion in alkaline brines. This suggests that corrosion models based on bulk solution experiments over the appropriate composition, temperature, and relative humidity range can be used to predict corrosion in thin brine films formed by salt deliquescence.

In contrast to the above-boiling period, the below-boiling period is characterized by predominately by NaCl based brines with minor amounts of K, NO_3, Ca, Mg, F, and Br at less than 70% relative humidity. These brines are identified as sulfate and bicarbonate brines by the chemical divide theory. Nitrate to chloride ratios are strongly tied to relative humidity and halite solubility. Once the relative humidity is low enough to produce brines saturated with respect to halite, then NO_3:Cl increases to levels, which may inhibit corrosion. In addition to the more abundant NaCl-based brines some measured pore waters will evaporate towards acid NaCl-$CaCl_2$ brines, which are potentially more corrosive than the other brine types. Acid volatility also occurs with this brine type, possibly indicating that chemical transformations may be important in thin films. In contrast to the above-boiling period, comparison of our experimental data with predicted data show that current geochemical YMP models adequately model in-drift chemistry in the below-boiling period.

References

Alai, M., Sutton, M., and Carroll, S. (2005) Evaporative Evolution of Brines from Synthetic Topopah Spring Tuff Pore Water, Yucca Mountain, NV. *Geochemical Transactions* (in press), UCRL-JRNL-206367.

Archer, D. G. (2000) Thermodynamic properties of the $NaNO_3$+H_2O System. *J Physical Chemistry. Ref. Data*, **29**, 1141-1156.

Blucher, D. B., Svensson, J.E., Johansson, L.G. (2003) The NaCl-Induced Atmospheric Corrosion of Aluminum; The Influence of Carbon Dioxide and Temperature. *J. Electrochemical Society*, **150**, B93-B98.

BSC (Bechtel SAIC Company) (2004a) Environment on the Surfaces of the Drip Shield and Waste Package Outer Barrier. ANL-EBS-MD-000001 REV 01. Las Vegas, Nevada.

BSC (Bechtel SAIC Company) (2004b) In-Drift Precipitates/Salts Model. ANL-EBS-MD-000045 REV 02. Las Vegas, Nevada: Bechtel SAIC Company.

BSC (Bechtel SAIC Company) (2004c) GENERAL CORROSION AND LOCALIZED CORROSION OF WASTE PACKAGE OUTER BARRIER (DC# 38358), ANL-EBS-MD-000003 REV 2.

Carroll, S. A., Staggs, K., and Gdowski, G. (2004) Deliquescence of Na-K-Cl-NO_3 salt mixtures up to 180˚C using resistivity techniques. Lawrence Livermore National Laboratory, UCRL-TR-207919-DRAFT

Carroll, S. A., Craig, L., and Wolery, T. (2005) Deliquescence of NaCl-$NaNO_3$, KNO_3-$NaNO_3$ and NaCl-KNO_3 salt mixtures from 90 to 120˚C. *Geochemical Transactions*, **6**, 19-30.

CRC Handbook, (1970-71), 51st ed., p.B-106.

Drever, J.I. (1997) The Geochemistry of Natural Waters: Surface and Groundwater Environments, 3rd Edition. Prentice Hall, New Jersey.

Eary, E.L. (1998). Predicting the effects of evapoconcentration on water quality in mine pit lakes. *Journal of Geochemical Exploration* **64**, 223-236.

Eugster, H.P. and Hardie, L.A. (1978) Saline lakes, In: Lerman, A. (Ed.), Lakes: Chemistry, Geology, Physics. Springer-Verlag, New York.

Falk,T., Svensson, J.E., Johansson, L.G. (1998) The Influence of CO_2 and NaCl on the Atmospheric Corrosion of Zinc, *J. Electrochemical Society*, **145**, 2993-2999.

Ge, Z., Wexler, A.S., and Johnston, M.V. (1998) Deliquescence behavior of multicomponent aerosols. *Journal of Physical Chemistry A*, **102**, 173-180

Hailey, P. and Gdowski, G. (2002) Thermogravimetric Thin Aqueous Film Corrosion Studies of Alloy 22; Calcium Chloride Solutions at 150°C and Atmospheric Pressure, *Materials Research Society Symposium Proceedings*, **757,** 765-770.

Helgeson, H.C., Delany, J.M., Nesbitt, H.W., and Bird, D.K. (1978) Summary and critique of the thermodynamic properties of rock-forming minerals. *Am. J. Sci.* **278-A**.

Holmes, H. F., Busey, R. H. Simonson, J. M, and Mesmer, R. E. (1987) The Enthalpy of dilution of HCl(aq) to 648 K and 40 MPa.. *J. Chem. Thermodynamics*, **19**, 863-890.

Holmes, H. F. and Mesmer, R. E. (1998) An isopiestic study of aqueous solutions of the alkali metal bromides at elevated temperatures. *J. Chem. Thermodynamics*, **30**, 723-741.

Kracek, F. C. (1928) P-T-X relations for systems of two or more components and containing two or more phases (L-V), (L_I,L_{II}-V and S-L-V systems), International Critical Tables of Numerical Data, Physics, Chemistry and Technology (ed. E. Washburn), **3**, 351-374.

Leygraf, C. (2000). Atmospheric corrosion. New York : Wiley-Interscience, 354 p.

Lindstrom, R., Johansson, L.G., Thompson, G.E., Skeldon, P., Svensson, J.E. (2004) Corrosion of Magnesium in Humid Air. *Corrosion Science,* **46**, 1141-1158.

Linke, W. F. (1965) Solubilities: Inorganic and Metal-Organic Compounds. V. 2, K-Z. 4th Edition, Washington, D. C., American Chemical Society, 250p.

Møller, N. (1988) The prediction of mineral solubility in natural waters: A chemical equilibrium model for the Na-Ca-Cl-SO_4-H_2O system to high temperature and concentration. *Geochim. Cosmochim. Acta*, **52**, 821-837.

Nguyen Q. A., Hailey P., Sutton M., Staggs K., Alai M., and Carroll S. A. (2003) Evaporative Concentration of 100x J13 Ground Water at 60% Relative Humidity and 90˚C, Lawrence Livermore National Laboratory, UCRL-TR-201284.

Pitzer, K. S., Peiper, J. C., and Busey, R. H. (1984). Thermodynamic properties of aqueous sodium chloride solutions. *J. Phys. Chem. Ref. Data*, **13**, 1-102.

Pitzer, K. S. (1991) Ion interaction approach: Theory and data correlation. In: K. S. Pitzer, (Editor) Activity Coefficients in Electrolyte Solutions, 2nd. Ed, CRC Press: Boca Raton, FL, pp. 75–153.

Pulvirenti, A.L., Needham, K.M., Adel-Hadadi, M.A., Bishop, E.J., Barkatt, A., Marks, C.R., Gorman, J.A. (2003) Effects of Volatilization on Groundwater Chemistry. *Mat. Res. Soc. Symp. Proc*., 587-593.

Rard, J. A. and Wijesinghe, A. M. (2003) Conversion of parameters between different variants of Pitzer's ion-interaction model, both with and without ionic strength dependent higher-order terms. *J. Chemical Thermodynamics*, **35**, 439–473.

Rard, J. A. (2004) Results from Boiling Temperature Measurements for Saturated Solutions in the Systems NaCl + KNO_3 + H_2O, $NaNO_3$ + KNO_3 + H_2O, and NaCl + $NaNO_3$ + KNO_3 + H_2O, Lawrence Livermore National Laboratory, UCRL-TR-207054.

Rosenberg, N.D., Gdowski, G. E., and Knauss K.G. (2001) Evaporative chemical evolution of natural waters at Yucca Mountain, Nevada. *Applied Geochemistry* **16**, 1231-1240.

Sutton, M., Alai, M. and Carroll, S. A. (2004) Evaporative Evolution of Carbonate-Rich Brines from Synthetic Topopah Spring Tuff Pore Water, Yucca Mountain, NV. *Mat. Res. Soc. Symp. Proc*. **824**, 497-502.

Vernon, W.H.J. (1932) *J. Institute of Metals*, **48**, 121.

Wolery, T. J. and Jarek, R. L. (2003) EQ3/6, Version 8.0, Software User's Manual, Software Document Number: 10813-UM-8.0-00, U.S. Department of Energy, Office of Civilian Radioactive Waste Management, Office of Repository Development, 1261 Town Center Drive, Las Vegas, Nevada 89144.

Yang, L., Pabalan, R. T., Browning, L. (2002) Experimental determination of the deliquescence relative humidity and conductivity of multicomponent salt mixtures. *Mat. Res. Soc. Symp. Proc*. **713**, 135-1422.

Yang, I. C., Rattray, G. W., Yu, P. (1996) Interpretation of Chemical and Isotopic Data from Boreholes in the Unsaturated Zone at Yucca Mountain, Nevada. USGS Water Resources Investigation Report 96-4058. US Geological survey, Denver, CO.